Monthly Notices
of the
ROYAL ASTRONOMICAL SOCIETY

MNRAS **460,** 1270–1299 (2016)
Advance Access publication 2016 March 21

doi:10.1093/mnras/stw641

The Dark Energy Survey: more than dark energy – an overview

Dark Energy Survey Collaboration: T. Abbott,[1] F. B. Abdalla,[2] J. Aleksić,[3] S. Allam,[4] A. Amara,[5] D. Bacon,[6] E. Balbinot,[7] M. Banerji,[8,9] K. Bechtol,[10,11] A. Benoit-Lévy,[2,12,13] G. M. Bernstein,[14] E. Bertin,[12,13] J. Blazek,[15] C. Bonnett,[16] S. Bridle,[17] D. Brooks,[2] R. J. Brunner,[18,19] E. Buckley-Geer,[4] D. L. Burke,[20,21] G. B. Caminha,[22,23] D. Capozzi,[6] J. Carlsen,[6] A. Carnero-Rosell,[24,25] M. Carollo,[26] M. Carrasco-Kind,[19,27] J. Carretero,[3,28] F. J. Castander,[28] L. Clerkin,[2] T. Collett,[6] C. Conselice,[29] M. Crocce,[28] C. E. Cunha,[20] C. B. D'Andrea,[6] L. N. da Costa,[24,25] T. M. Davis,[30] S. Desai,[32,31] H. T. Diehl,[4] J. P. Dietrich,[32,31] S. Dodelson,[4,33,34] P. Doel,[2] A. Drlica-Wagner,[4] J. Estrada,[4] J. Etherington,[6] A. E. Evrard,[35,36] J. Fabbri,[2] D. A. Finley,[4] B. Flaugher,[4] R. J. Foley,[18,27] P. Fosalba,[28] J. Frieman,[4,34] J. García-Bellido,[37] E. Gaztanaga,[28] D. W. Gerdes,[35] T. Giannantonio,[8,9] D. A. Goldstein,[38,39] D. Gruen,[20,21] R. A. Gruendl,[19,27] P. Guarnieri,[6] G. Gutierrez,[4] W. Hartley,[5] K. Honscheid,[15,40] B. Jain,[14] D. J. James,[1] T. Jeltema,[41] S. Jouvel,[2] R. Kessler,[33,34] A. King,[30] D. Kirk,[2] R. Kron,[33] K. Kuehn,[42] N. Kuropatkin,[4] O. Lahav,[2]★ T. S. Li,[43] M. Lima,[25,44] H. Lin,[4] M. A. G. Maia,[24,25] M. Makler,[22] M. Manera,[2] C. Maraston,[6] J. L. Marshall,[43] P. Martini,[15,45] R. G. McMahon,[8,9] P. Melchior,[46] A. Merson,[2] C. J. Miller,[35,36] R. Miquel,[3,38] J. J. Mohr,[32,47,31] X. Morice-Atkinson,[6] K. Naidoo,[2] E. Neilsen,[4] R. C. Nichol,[6] B. Nord,[4] R. Ogando,[24,25] F. Ostrovski,[8,9] A. Palmese,[2] A. Papadopoulos,[6,48] H. V. Peiris,[2] J. Peoples,[4] W. J. Percival,[6] A. A. Plazas,[49] S. L. Reed,[8,9] A. Refregier,[5] A. K. Romer,[50] A. Roodman,[20,21] A. Ross,[15] E. Rozo,[51] E. S. Rykoff,[20,21] I. Sadeh,[2] M. Sako,[14] C. Sánchez,[3] E. Sanchez,[52] B. Santiago,[53,25] V. Scarpine,[4] M. Schubnell,[35] I. Sevilla-Noarbe,[27,52] E. Sheldon,[54] M. Smith,[55] R. C. Smith,[1] M. Soares-Santos,[4] F. Sobreira,[4,25] M. Soumagnac,[2] E. Suchyta,[14] M. Sullivan,[55] M. Swanson,[56] G. Tarle,[35] J. Thaler,[18] D. Thomas,[6,57] R. C. Thomas,[58] D. Tucker,[4] J. D. Vieira,[18,19,27] V. Vikram,[59] A. R. Walker,[1] R. H. Wechsler,[20,21] J. Weller,[31,47,60] W. Wester,[4] L. Whiteway,[2] H. Wilcox,[6] B. Yanny,[4] Y. Zhang[35] and J. Zuntz[17]

Affiliations are listed at the end of the paper

Accepted 2016 March 14. Received 2016 January 22; in original form 2016 January 22

ABSTRACT

This overview paper describes the legacy prospect and discovery potential of the Dark Energy Survey (DES) beyond cosmological studies, illustrating it with examples from the DES early data. DES is using a wide-field camera (DECam) on the 4 m Blanco Telescope in Chile to image 5000 sq deg of the sky in five filters (*grizY*). By its completion, the survey is expected

★ E-mail: o.lahav@ucl.ac.uk

to have generated a catalogue of 300 million galaxies with photometric redshifts and 100 million stars. In addition, a time-domain survey search over 27 sq deg is expected to yield a sample of thousands of Type Ia supernovae and other transients. The main goals of DES are to characterize dark energy and dark matter, and to test alternative models of gravity; these goals will be pursued by studying large-scale structure, cluster counts, weak gravitational lensing and Type Ia supernovae. However, DES also provides a rich data set which allows us to study many other aspects of astrophysics. In this paper, we focus on additional science with DES, emphasizing areas where the survey makes a difference with respect to other current surveys. The paper illustrates, using early data (from 'Science Verification', and from the first, second and third seasons of observations), what DES can tell us about the Solar system, the Milky Way, galaxy evolution, quasars and other topics. In addition, we show that if the cosmological model is assumed to be Λ+cold dark matter, then important astrophysics can be deduced from the primary DES probes. Highlights from DES early data include the discovery of 34 trans-Neptunian objects, 17 dwarf satellites of the Milky Way, one published $z > 6$ quasar (and more confirmed) and two published superluminous supernovae (and more confirmed).

Key words: surveys – minor planets, asteroids: general – supernovae: general – Galaxy: general – galaxies: general – quasars: general.

1 INTRODUCTION

Many ongoing and planned imaging and spectroscopic surveys aim at measuring dark energy (DE) and other cosmological parameters. However, these surveys map huge volumes of the cosmos and they can be used to study many other astrophysical objects and phenomena. Here we focus on the Dark Energy Survey (DES),[1] illustrating its power with the early 'Science Verification' (SV),[2] first year (Y1), second year (Y2) and third year (Y3) data. We consider non-cosmology science derived in two ways: (i) science outside the original scope of DES: the Solar system, the Milky Way, galaxy evolution, quasars (QSOs) and transients; and (ii) astrophysics resulting from cosmology probes if the cosmology is already assumed, say to be Λ+cold dark matter (LCDM). The motivation here is to emphasize where DES data make a difference with respect to current data, rather than to cover everything one can do with DES. This paper illustrates science with DES alone, as well as in combination with other data sets, methods used and DES applications for the future. This paper aims to present DES to a wide readership. First, for those who will be using data from the DES public archive, this paper demonstrates what can be done with the public data.[3] Secondly, this paper targets those who are applying for community observing time on the Dark Energy Camera (DECam), in providing ideas about the system's capabilities. Thirdly, this paper could be of interest to those conducting current and future imaging and spectroscopic surveys, e.g. the Hyper Suprime-Cam,[4] the Kilo-Degree Survey,[5] the Large Synoptic Survey Telescope (LSST),[6] *Euclid*,[7] the Wide-Field Infrared Survey Telescope (WFIRST), the Subaru Prime Focus Spectrograph (PFS),[8] the Dark Energy Spectroscopic Instrument (DESI)[9] and 4MOST.[10]

White (2007) made the point that there is a risk that DE-motivated projects may focus too strongly on a single science question. This paper is partly intended to demonstrate that even if a project is optimized for DE searches, it can and does have numerous spin-offs, including some well beyond cosmology. It is anticipated that the next generation of DE-inspired projects (e.g. LSST, DESI, *Euclid*, WFIRST) will also have such legacy value.[11]

The outline of this paper is as follows. Section 2 summarizes the DES survey, its properties, and an inventory of objects recorded so far and expected from the full survey. Sections 3 to 11 are ordered by the proximity of objects to the Earth, and cover the Solar system, the Milky Way, galaxy evolution (including galaxy biasing and intrinsic alignments), clusters, strong lensing, quasars, supernovae (SNe) and the follow-up of gravitational wave (GW) alerts. The last section summarizes the results, and forecasts what legacy science DES is likely to yield after completing its five seasons.

2 THE DARK ENERGY SURVEY

DES is an imaging survey of 5000 sq deg of the southern sky, using a 570 megapixel camera on the Cerro Tololo Inter-American

[1] http://www.darkenergysurvery.org/
[2] For public data release see http://des.ncsa.illinois.edu/releases/sva1
[3] In addition to raw survey images released through the NOAO Science Archive (NSA) 12 months after they are taken, reduced, calibrated images processed through the DES Data Management (DESDM) system are being made publicly available through the NSA. In addition, DES will make two public releases of co-added images and catalogues produced and served by DESDM, one based on the first two seasons of data, and the second based on the full survey data set.
[4] http://www.naoj.org/Projects/HSC/
[5] http://kids.strw.leidenuniv.nl/
[6] http://www.lsst.org/
[7] http://www.euclid-ec.org/
[8] http://pfs.ipmu.jp/factsheet/
[9] http://desi.lbl.gov/
[10] http://www.4most.eu/
[11] A companion DES overview paper (in preparation) will describe the survey and the DES project in more detail, as well as cosmological studies such as DE, dark matter (DM) and other cosmological properties, e.g. cosmological parameters from early DES weak lensing data (Dark Energy Survey Collaboration 2015) and forecast for neutrino mass from DES large-scale structure (Lahav et al. 2010).

Observatory (CTIO) 4 m Blanco Telescope in Chile. Photometric redshifts are obtained from the multiband photometry to produce a quasi-three-dimensional survey. The main goal of DES is to determine the DE equation of state w (the ratio of pressure to density) and other key cosmological parameters to high precision. DES will measure w using complementary techniques in a single survey: counts of galaxy clusters, weak gravitational lensing and galaxy power spectra. DES is expected to catalogue 300 million galaxies with photometric redshifts; 200 million of them will have shape measurements for weak lensing. In addition, thousands of Type Ia supernovae (SNe Ia) will be measured in 27 sq deg 'time-domain' fields. It is expected that the uncertainty on w will be only a few per cent for each probe. See Dark Energy Survey Collaboration (2005) and a companion overview paper (DES Collaboration, in preparation) for detailed parametrizations and statistics.

DES is an international collaboration, with over 400 scientists from the US, the UK, Spain, Brazil, Germany, Switzerland and Australia. The DES science is coordinated by a Science Committee comprised of 13 Science Working Groups (SWGs). Core DE SWGs include LSS, clusters, weak lensing and SNe Ia. Additional SWGs which focus on the primary science are photometric redshifts, spectroscopy, simulations, and theory and combined probes. The non-DE SWGs focus on Milky Way science, galaxy evolution, strong lensing, quasars, and transients and moving objects.

The DES footprint is shown in Fig. 1, and Table 1 presents an inventory of measured and discovered objects so far (2015 December), as well as forecast for the complete survey. The first light of DES was obtained in 2012 September, followed by commissioning of DECam (Flaugher et al. 2015). SV observations took place from 2012 November 2012 to 2013 February, and the Y1 and Y2 observations were taken from 2013 August to 2014 February, and from 2014 August to 2015 February, respectively. The SV data cover about 250 sq deg to nearly the full DES depth, in part overlapping the South Pole Telescope (SPT) area, as well as some SN fields. Analyses presented below have used different subsets of the SV data. Five optical filters (*grizY*) were used throughout the SV, with typical single exposure times of 90 s for *griz* and 45 s for *Y*. Details of the resulting magnitude limits from the SV season in the wide survey in each band (nominally for 10 exposures, but in practice fewer) are shown in Table 2. For the depth obtained during SV with the SN fields, see Sánchez et al. (2014).

Separation of stars and galaxies in the SV data was done using a number of codes, resulting in a galaxy purity of 98 per cent and completeness of 80 per cent down to $i = 22.5$ (Crocce et al. 2016). See more in Soumagnac et al. (2015) for star/galaxy separation methodology for DES. The performance of several photo-z methods applied to SV data was evaluated in Sánchez et al. (2014). The best methods yielded scatter $\sigma_{68} = 0.08$ (defined as the 68 per cent width about the median of $\Delta z = z_{\rm spec} - z_{\rm phot}$). Regarding the image quality, the achieved median seeing full width at half-maximum is about 0.9 arcsec in filters *riz*, as expected when designing the survey for weak lensing analyses. The shape measurements (using two methods) for about 3 million SV galaxies are presented in Jarvis et al. (2015), who conclude that the shear is determined with multiplicative errors of ± 5 per cent (1σ). The 27 sq deg (over 10 fields) that comprise the SN survey (Bernstein et al. 2012) are observed in the *griz* bands at approximately weekly intervals throughout each six-month DES observing season, and provide a much more densely sampled time series.

Although observed for testing purposes, SV is a powerful data set in its own right, particularly for weak lensing, where it rivals the full CFHTLenS survey for size (though DES SV is slightly shallower). By design, there is significant overlap with the SPT survey (see Fig. 1 for overlapping surveys). The SV phase of DES was recently combined with near-infrared data from ESO's VISTA Hemisphere Survey (VHS), described in McMahon et al. (2013) and Banerji et al. (2015), which was used to extract fluxes and associated errors from the shallower VHS data. Joint seven-band (*grizYJK*) photometric catalogues were produced for a single 3 sq deg DECam field, where the multiwavelength photometry and spectroscopy were used for data quality tests. This will be extended to the full DES+VHS when the survey is complete. We also note the synergy with the Australian OzDES, a 100-night spectroscopic survey with the 2dF fibre-fed spectrometer on the Anglo-Australian Telescope dedicated to following up DES targets identified in the SN fields (Yuan et al. 2015).

The Y1 and Y2 observations (now complete) aimed at covering most of the 5000 sq deg footprint to about 40 per cent of the final survey depth. Single-epoch data of Y1 and Y2 have already been used in searches for new Milky Way companions (Bechtol et al. 2015; Drlica-Wagner et al. 2015b). Catalogues are currently being prepared for studies of LSS, clusters and weak lensing. As shown in Table 1, the Y1 and Y2 catalogues will yield 100M galaxies with photo-z, of which 80M will have shape measurements for weak lensing studies.

The collaboration also prepared a set of Data Challenge simulations (Data Challenge 6, BCC, MICE), which are being analysed alongside the real data as explained below. The simulations are described in other collaboration papers.

3 SOLAR SYSTEM SCIENCE WITH DES

DES was designed to have a combination of area and depth optimized for extragalactic astronomy and cosmology. To achieve the deep co-added images required for cosmological measurements, the same fields are repeatedly observed over the 5 years of the survey. This survey strategy also gives DES the ability to detect moving transients over $\sim 1/8$ of the sky, making it a uniquely powerful tool for observation and discovery within the Solar system.

The ability to detect Solar system transients is a function of both the single-epoch exposure depth and the observing cadence, as well as the rate of motion of the object through the survey area. Most Solar system objects follow orbits within $\pm 20^\circ$ of the ecliptic plane. Higher inclination objects have typically experienced at least one scattering event, and their dynamics encodes the history of such encounters. Fig. 1 shows the wide survey and SN fields in relation to the ecliptic plane. The equatorial stripe encompasses approximately 500 sq deg within 20 deg of the ecliptic. Five of the SN fields also lie at moderate ecliptic latitudes. The bulk of the survey area, however, lies at ecliptic latitudes below -20°. This region is seldom covered by surveys that explicitly target Solar system objects – for example the 'other' DES, the Deep Ecliptic Survey (Millis et al. 2002) – but makes *this* DES particularly sensitive to unusual high-inclination objects, such as Centaurs and members of the distant scattered disc.

We illustrate the capabilities of DES with a discussion of four types of Solar system objects: near-earth objects (NEOs), main belt asteroids, distant objects including Trojans and Centaurs, and the trans-Neptunian region.

3.1 Near-earth objects

NEOs move rapidly and are often observed over arc lengths of only a few days. For this reason, their positional uncertainty can grow rapidly, and many newly detected NEOs soon become undetectably

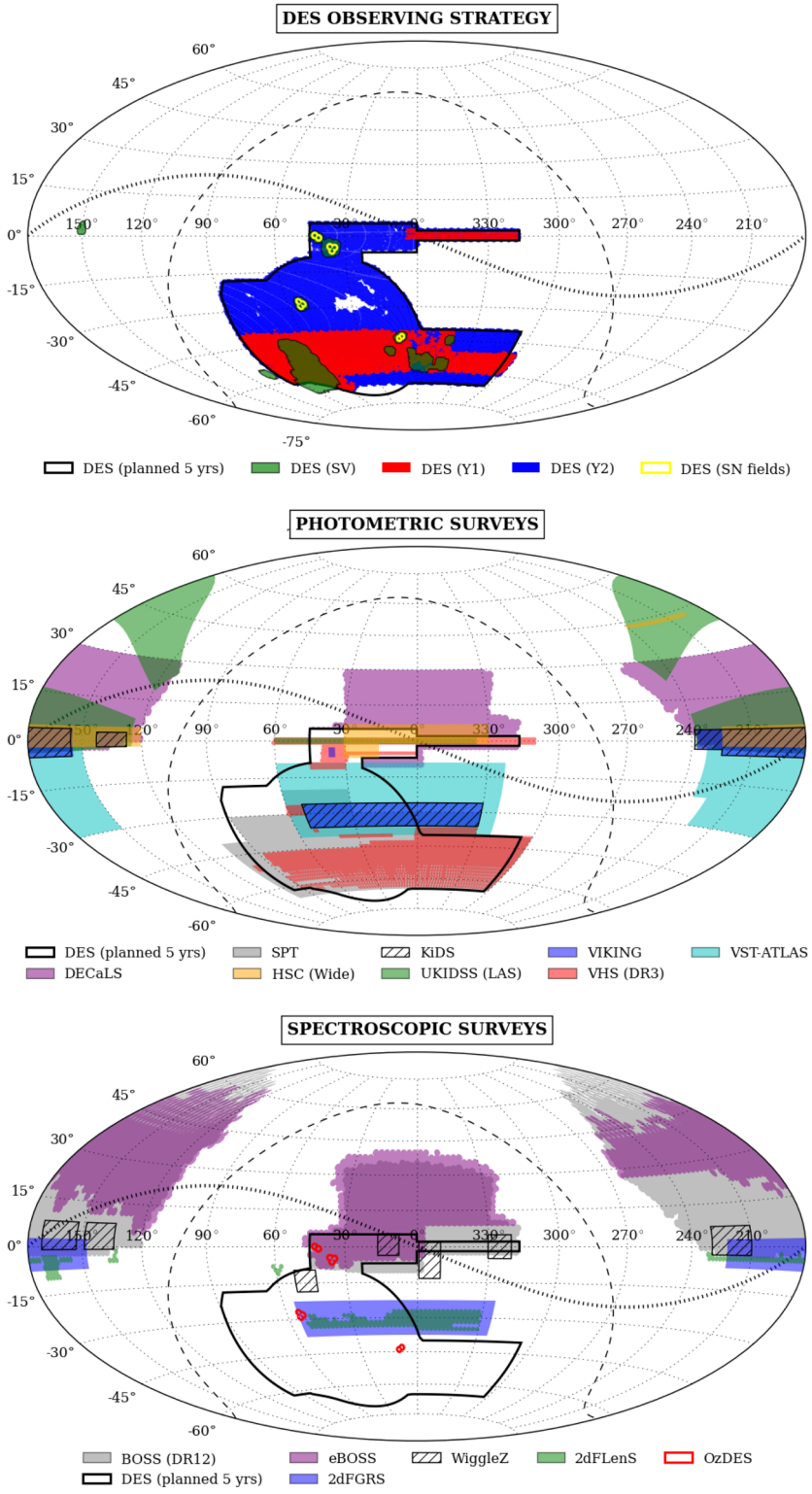

Figure 1. DES and some selected completed or ongoing surveys (as of 2015 December). This is a Hammer projection in equatorial coordinates, with the dashed and dotted lines indicating the Galactic plane and the ecliptic plane, respectively. Top: DES survey footprint for the SV, Y1, Y2 and the final 5 yr survey. Middle: with other photometric surveys. Bottom: with other spectroscopic surveys. Planned wide-field surveys not shown include LSST and WFIRST (both photometric), *Euclid* (photometric and spectroscopic), Sumire PFS, DESI and 4MOST (all three spectroscopic). We note the VHS (DR3) indicates deep coverage in the DES area. Eventually, it will cover nearly the whole of the DES 5 yr footprint. A shallower VISTA whole hemisphere is also underway. The DES footprint was designed to have large overlap with SPT (shown here in the 'photometric surveys' plot). DES SV and Y1 areas essentially completely overlap SPT, and the full planned DES overlaps the completed 2500 sq deg SPT.

Table 1. The current DES inventory: different objects observed with DES over the SV, Y1 and Y2 seasons, and the expectation for the full five seasons. σ for galaxies and stars indicates signal/noise ratio, and λ for clusters denotes richness.

Objects	As of 2015 December	Expected from full 5 yr DES
Galaxies with photo-z ($>10\sigma$)	7M (SV), 100M (Y1+Y2)	300M
Galaxies with shapes	3M (SV), 80M (Y1+Y2)	200M
Galaxy clusters ($\lambda > 5$)	150K (Y1+Y2)	380K
SN Ia	1000	Thousands identified photometrically
Superluminous SN	2 (published) + more confirmed spectroscopically + many more candidates	15–20
New Milky Way companions	17	25
QSOs at $z > 6$	1 (published) + more confirmed spectroscopically + many more candidates	375
Lensed QSOs	2	100 ($i < 21$)
Stars ($>10\sigma$)	2M (SV), 30M (Y1+Y2)	100M
Solar system: new trans-Neptunian objects	32 in SN fields + 2 in the WF	50 + many more in the wide field
New Jupiter Trojans	19	
Main belt asteroids	300K (Y1+Y2)	
Kuiper belt objects		500–1000

Table 2. Estimated PSF magnitude limits from a subset of the DES SV data, based on Balrog simulations embedded into 210 sq deg of the DES imaging (see Suchyta et al. 2016). We calculate the S/N versus magnitude response in tiles of approximately 0.5 sq deg, identify the S/N = 10 magnitude value in each tile, then compute the median of these values. The estimation is for objects simulated as point sources (regardless of their measured classification as stars or galaxies). The DES SV survey mimicked the full 5 yr DES survey (ideally of 10 exposures), but with significant depth variations due to weather and other challenges during early operations of DECam (see e.g. Leistedt et al. 2015), so effectively less than 10 exposures. Overall, the Blanco and DECam performance has improved considerably after SV.

Band	Nominal SV exposures	mag (10σ)
g	10×90 s	24.45
r	10×90 s	24.30
i	10×90 s	23.50
z	10×90 s	22.90
Y	10×45 s	21.70

faint as they recede from Earth and hence are lost. DECam's depth and 3 sq deg field of view make it an excellent instrument for NEO detection and recovery. DES has performed target-of-opportunity observations of a handful of NEOs, such as the recovery of the potentially hazardous asteroid 2014 BE_{63}. A programme to search for NEOs with DECam is underway using community time (Allen et al. 2014).

3.2 Main belt asteroids

The vast majority of known asteroids occupy the main asteroid belt between Mars and Jupiter. As of 2015 January 6, the Minor Planet Center[12] (MPC) lists over 650 000 objects with semi-major axes between 2 and 4 au. By comparing the calculated positions and magnitudes of these asteroids with the ≈40 000 DES wide and SN survey exposures from the Y1 and Y2 observing seasons, we estimate that approximately 70 000 known main belt asteroids should already have been observed by DES, with detected objects being visible in a median of six exposures at a median magnitude of 20.5. Hence, DES can already provide useful information about a large number of main belt asteroids.

[12] http://www.minorplanetcenter.net

However, the catalogues of known Solar system objects are very incomplete at the DES exposure depth. To illustrate this, the left-hand panel of Fig. 2 shows the motion, in arcseconds per hour, of moving transients detected in a single exposure sequence in the deep SN field X3 on 2013 September 24. This sequence consisted of five consecutive 360 s i-band exposures. 73 moving transients were detected in this sequence, of which only 13 were matched to known main belt asteroids. The rate of retrograde motion of the unmatched population is consistent with the known objects, suggesting that they are also main belt asteroids. There is, however, an excess of unmatched objects with somewhat lower motions. Several of the latter objects have been observed in images taken during other epochs and confirmed as Trojan companions of Jupiter.

Though still at an early stage, the search for main belt asteroids with DES should eventually lead to hundreds of thousands of new detections. Linking single-night observations of new main belt objects into orbits poses a challenge, however, because the DES wide-survey observing cadence is not well matched to these objects' relatively high rates of motion. There is currently no plan within DES to attempt orbit-linking for main belt asteroids, but we intend to submit all detected moving transients to the MPC, where links may be made to current or future data from other surveys.

3.3 Distant Solar system objects

The Solar system beyond the main belt contains several distinct groups of minor planets.

(i) The Trojan populations of Jupiter and Neptune, consisting of objects in a stable 1:1 mean motion resonance centred upon the leading (L4) or trailing (L5) Lagrange points of their parent body.

(ii) Centaurs, with chaotic orbits that cross the orbits of the giant planets. Believed to be objects ejected from the Kuiper belt, Centaurs evolve along complicated dynamical pathways that may end in capture as a Jupiter-family comet, collision with a giant planet or with the Sun or even ejection from the Solar system.

(iii) The trans-Neptunian region, with a rich dynamical structure that includes the classical Kuiper belt, various mean motion Neptunian resonances, the scattered disc and a small but very interesting group of detached/inner Oort cloud objects with perihelia greater than 50 au (such as the dwarf planet Sedna). An early indication of the power of DECam came with the discovery by Trujillo & Sheppard (2014) of a second Sedna-like object, 2012 VP_{113}, whose perihelion of 80.3 au is the largest known.

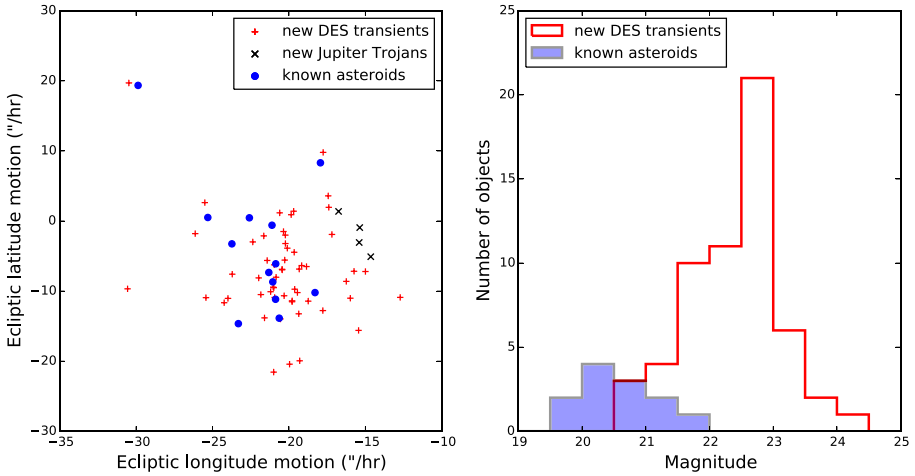

Figure 2. Properties of transients observed in a single visit to the DES-SN search field X3, consisting of five 360 s *i*-band exposures on 2013 September 24. Left: hourly motion in ecliptic latitude and longitude, with objects matched to previously known main belt asteroids indicated. The new DES detections include several Jupiter Trojans that are among 19 such objects found by DES to date. Right: comparison of magnitudes of previously known objects with new DES detections. The known asteroids have a median *i*-band magnitude of 20.5, compared to a median of 22.6 for the new DES objects.

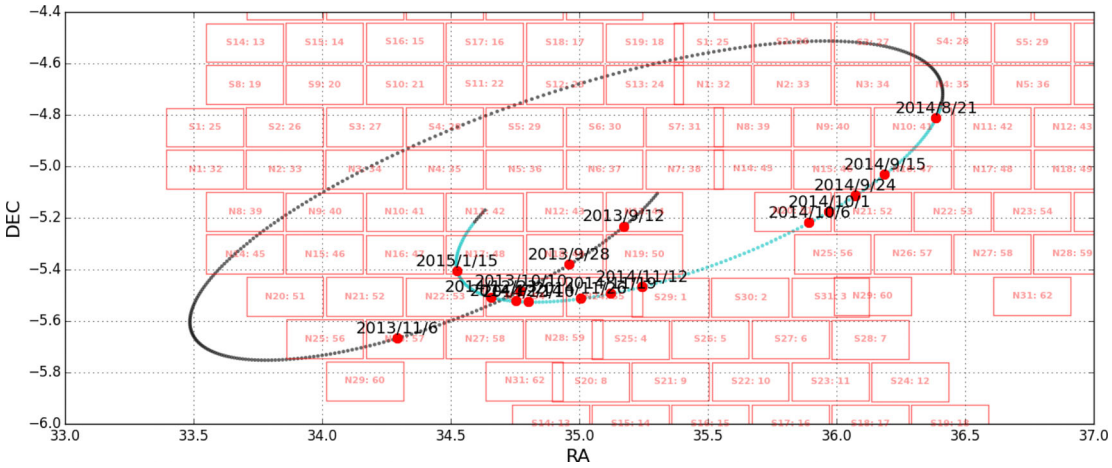

Figure 3. Trajectory of the plutino 2013 RD_{98} through three adjacent SN fields during the DES Y1 and Y2 seasons. Large dots indicate nights on which the object was observed by DES. Each rectangle represents one DECam CCD.

To date the search for trans-Neptunian objects (TNOs) with DES has been carried out in the 10 SN fields using the full Y1 and Y2 data samples, as well as the Y3 data up through 2015 October. These fields encompass 27 sq deg, less than 1 per cent of the full wide-survey area, but are an excellent starting point for the TNO search because they are observed with a one-week nominal cadence in the *griz* bands throughout each six-month DES observing season. Five of the fields are at moderate ecliptic latitudes of −15 to −20 deg, while the other five are at higher latitudes of around −45 deg. The search begins with the list of transient candidates identified in each single-epoch exposure using the SN difference-imaging pipeline (Kessler et al. 2015). Artefacts and other non-point-like detections are removed with the Autoscan machine-learning algorithm of Goldstein et al. (2015). The apparent motion of a TNO is dominated by earth-reflex motion; for example an object at 40 au observed near opposition will undergo retrograde motion at 3–4 arcsec h^{-1}. This allows us to identify candidate triplets of points – the minimum number required for an orbital solution – from nearby visits to a given field, separated in a way consistent with seasonally appropriate reflex motion. We attempt to fit each triplet to an orbit using the `fit_radec` algorithm of Bernstein & Khushalani (2000). With a successful candidate orbit in hand, the two-week arc of a typical triplet can be readily extended to include points from subsequent or prior visits, into adjacent fields including possible wide-survey detections, and into different DES observing seasons. The trajectory of one such object is shown in Fig. 3.

The search for TNOs in the DES-SN fields has yielded 32 new objects through the first part of Y3. Their orbital elements and other properties are listed in Table 3. Due to the location of our search fields, all have inclinations of at least 15°, increasing the population of known 'hot' TNOs by about 10 per cent. Fig. 4 shows the inclination versus semi-major axis for these new objects, while Fig. 5 shows absolute magnitude as a function of solar distance at discovery. From this figure, one can read off the sensitivity of DES to larger, more distant objects; e.g. with a magnitude depth of 24, DES could discover a $H = 5$ object (approximately 600 km in diameter) at 80 au, a distance comparable to the distance at discovery of the larger objects Sedna and 2012 VP_{113}. The DES discoveries include a number of objects in mean motion resonances with Neptune, as well as several distant scattered disc objects. In particular, we highlight the pair of L4 Neptune Trojans 2014 QO_{441} and 2014

Table 3. Barycentric osculating orbital elements and other properties of 32 distant Solar system objects discovered in the DES-SN fields. These data were retrieved from the MPC on 2015 November 20. Scattered disc objects (SDOs) and objects in mean motion resonances with Neptune are indicated in the last column.

Designation	a (au)	e	i (deg.)	Ω (deg.)	ω (deg.)	M (deg.)	Epoch	Peri. date	H	Comment
2012 VR_{113}	47.57	0.17	19.3	121.1	220.5	38.2	2015-06-27.0	1980-09-08	6.6	2:1 resonance
2012 VS_{113}	55.02	0.31	26.8	171.7	220.4	3.9	2015-06-27.0	2011-02-09	7.1	SDO
2012 VU_{113}	39.43	0.08	30.1	65.5	315.8	12.5	2015-06-27.0	2006-11-25	7.7	plutino
2012 VV_{113}	46.01	0.11	15.7	116.1	295.6	349.3	2015-06-27.0	2024-10-08	7.4	
2012 WD_{36}	76.52	0.51	23.7	177.4	293.9	336.8	2016-01-13.0	2059-03-02	6.9	
2012 YO_{9}	43.64	0.17	15.4	118.7	3.3	298.7	2015-06-27.0	2064-07-16	7.7	SDO
2013 QO_{95}	39.89	0.03	20.6	83.1	323.2	345.4	2015-06-27.0	2025-09-10	6.6	
2013 QP_{95}	40.57	0.17	25.4	71.4	19.5	314.5	2015-06-27.0	2048-03-01	7.2	11:7 resonance
2013 RB_{98}	42.17	0.26	22.0	147.2	350.6	286.5	2015-06-27.0	2071-06-02	6.6	5:3 resonance
2013 RD_{98}	39.36	0.23	19.6	145.0	104.0	126.2	2015-06-27.0	1928-11-14	7.3	plutino
2013 RF_{98}	325.1	0.89	29.6	67.6	316.5	0.1	2013-09-25.0	2011-11-18	8.6	SDO
2013 RG_{98}	23.22	0.17	46.0	146.0	350.3	291.6	2015-06-27.0	2036-10-01	9.0	Centaur
2013 SE_{99}	79.54	0.54	18.3	100.6	223.8	20.8	2015-06-27.0	1974-07-15	7.8	SDO
2013 TH_{159}	40.86	0.09	33.6	62.4	233.0	84.3	2015-06-27.0	1954-05-01	8.6	
2013 TV_{158}	111.24	0.67	31.2	181.1	232.3	357.8	2015-06-27.0	2022-08-22	6.3	SDO
2013 VD_{24}	54.51	0.24	18.9	105.7	196.8	62.6	2013-12-14.0	1943-12-16	7.7	SDO
2014 QL_{441}	48.36	0.25	26.3	75.8	293.5	11.6	2016-01-13.0	2005-03-25	6.5	
2014 QM_{441}	39.5	0.28	18.3	96.1	313.0	354.9	2016-01-13.0	2019-07-16	8.5	plutino
2014 QN_{441}	46.07	0.28	20.7	144.7	242.8	3.1	2015-06-27.0	2012-09-30	6.7	
2014 QO_{441}	30.06	0.11	18.8	107.1	112.5	169.9	2015-06-27.0	1937-09-12	8.2	Neptune Trojan
2014 QP_{441}	30.08	0.07	19.4	96.6	3.2	297.9	2014-10-30.0	2043-04-15	9.2	Neptune Trojan
2014 QR_{441}	67.45	0.37	42.2	77.9	283.0	354.6	2016-01-13.0	2024-04-18	6.8	SDO
2014 QS_{441}	46.76	0.06	38.0	186.0	257.2	316.6	2016-01-13.0	2054-07-19	5.6	
2014 QU_{441}	41.15	0.11	19.3	113.2	301.2	341.0	2016-01-13.0	2029-12-18	8.0	
2014 SB_{349}	25.82	0.18	15.5	117.2	359.2	300.4	2016-01-13.0	2037-10-01	9.5	Centaur
2014 SZ_{348}	48.07	0.23	47.7	158.6	239.6	6.9	2015-06-27.0	2009-02-12	8.0	
2014 TT_{85}	40.58	0.07	17.8	98.4	280.8	16.1	2014-10-30.0	2003-03-29	8.0	
2014 TU_{85}	48.65	0.31	16.4	120.8	306.1	340.9	2014-10-10.0	2032-10-21	8.4	
2014 UF_{224}	45.39	0.13	27.2	174.4	330.5	264.7	2015-06-27.0	2096-06-08	7.4	
2014 VT_{37}	39.95	0.26	33.5	197.7	175.6	18.6	2014-12-09.0	2001-11-25	9.0	plutino
2015 PD_{312}	54.54	0.36	23.1	155.0	243.7	356.9	2015-08-26.0	2019-01-26	8.1	SDO
2015 PF_{312}	45.39	0.1	18.0	160.9	208.3	24.1	2015-08-26.0	1995-02-22	6.3	

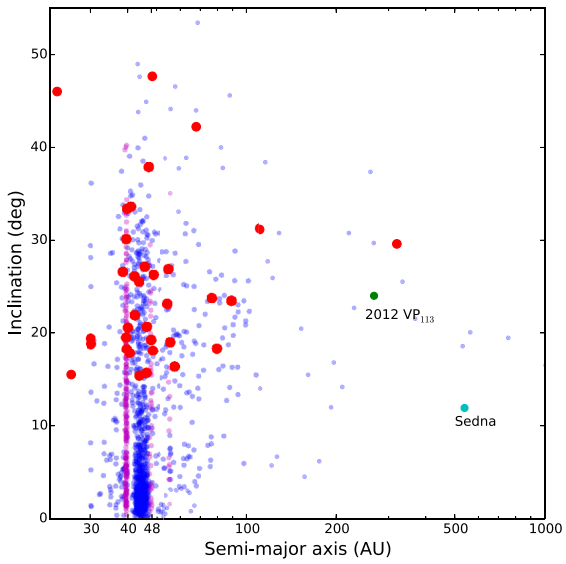

Figure 4. Inclination versus semi-major axis for 32 distant Solar system objects (large circles) discovered in the DES-SN fields. Small circles indicate other known TNOs. The band of objects at $a = 39.3$ au are plutinos in a 3:2 mean motion resonance with Neptune. The inner Oort cloud objects Sedna and 2012 VP_{113} are also indicated. Due to the location of the search fields, all of the new detections have inclinations of at least 15°.

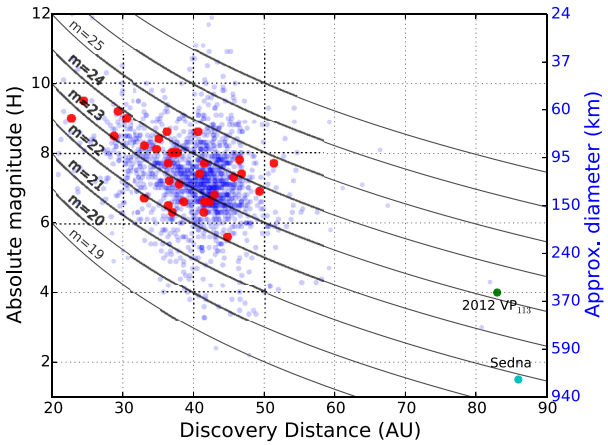

Figure 5. Absolute magnitude versus heliocentric distance at discovery for 32 distant Solar system objects (large circles) discovered in the DES-SN fields. Small circles indicate other known TNOs. The conversion from absolute magnitude to size assumes an albedo of 5 per cent. The inner Oort cloud objects Sedna and 2012 VP_{113} are also indicated.

QP_{441} (Gerdes et al. 2016), which raise the number of known stable Neptune Trojans to 12. We also highlight the 'extreme TNO' 2013 RF_{98}, whose 325 au semi-major axis is the fifth largest of any known Solar system object that does not cross the orbit of Neptune. 2013

RF_{98} and the other longest period TNOs display as-yet-unexplained clustering in the argument of perihelion near $\omega = 0^\circ$, which may result from a stabilizing interaction with a distant perturber (de la Fuente Marcos & de la Fuente Marcos 2014; Trujillo & Sheppard 2014). The minor planet 2013 RF_{98} is one of the six most distant TNOs whose aligned orbits were used by Batygin & Brown (2016) to hypothesize the existence of Planet 9. As the modelled trajectory of Plant 9 lies within the DES footprint, DECam would be ideal to search for it.

While the TNO search in the SN fields has already produced objects of interest and will continue to do so in the remaining years of the survey, it is ultimately the DES wide survey that will have the greatest potential to chart new territory in the trans-Neptunian region. With its combination of area, depth and a survey footprint weighted towards high ecliptic latitudes, DES has the potential to discover ∼30× more 'hot' TNOs than any previous survey. DES's high-latitude coverage compliments Sheppard and Trujillo's ongoing TNO search programme using DECam at lower ecliptic latitudes. Although little is known about the distribution of detached Sedna-like objects, it seems reasonable to suppose that they are less likely to lie close to the ecliptic plane than more typical TNOs. If so, DES has the potential to discover tens of such objects, making detailed studies of the population and dynamics of the inner Oort cloud possible for the first time.

4 STELLAR, MILKY WAY AND LOCAL GROUP SCIENCE

Wide-field photometric surveys have significantly expanded our understanding of the Milky Way and its stellar populations. For instance, the speed and depth of recent digital surveys have considerably improved the census of low-mass and low-luminosity stars and substellar objects (e.g. Kilic et al. 2006; Zhang et al. 2009). These surveys have also revealed complex substructure in the Galactic halo (e.g. Rocha-Pinto et al. 2004; Willman et al. 2005; Koposov et al. 2008; Walsh, Willman & Jerjen 2009; Sharma et al. 2010). Together, these data sets have allowed us to better characterize the structure, mass assembly and star formation history (SFH) of our Galaxy (e.g. Jurić et al. 2008; Reylé et al. 2009). With exceptional sensitivity over the southern Galactic cap, DES promises to further expand our knowledge of the local environment.

The purpose of this section is to address topics in stellar, Milky Way and Local Group science where the DES survey will provide important input. We will address topics in order of proximity to the Earth, starting with nearby Milky Way stellar populations and concluding with Local Group satellite galaxies. When possible, we will note topics that are already being studied with the early DES data sets. The list of topics cited here is almost certainly incomplete, and will likely be expanded as the full DES data set becomes available. Much of the work in this section builds on the studies of Rossetto et al. (2011); however, the DES footprint and projected photometric sensitivity have been subsequently refined.

4.1 A census of L and T dwarfs in the Galactic disc

A large number of substellar objects are necessary to infer the fundamental properties of brown-dwarf populations, such as their initial mass function (IMF). Unlike normal main-sequence (MS) stars, determining the masses of brown dwarfs requires both their luminosity and ages to be known, effectively coupling the determination of their IMF and SFH (Day-Jones et al. 2013a). The `Trilegal` Galactic model adopted by Rossetto et al. (2011) predicts that DES will observe $\sim 3 \times 10^4$ objects with $M \leq 0.08\,M_\odot$. This number is about an order of magnitude larger than the current census of known objects of substellar mass. Given the extremely low luminosities of these objects, they will be largely restricted to within one or two thin-disc scaleheights. It will be challenging to extract the sample of L and T dwarfs from the DES data, partly due to these objects being detectable only in the redder filters. Availability of the *Y* band will be helpful in disentangling them from the high-z galaxy and QSO populations, specifically based on their positions in $(z - Y)$ versus $(i - z)$ colour–colour diagrams. DES and VHS data can be combined to provide a more comprehensive fit to the spectral energy distributions (SEDs) of these objects.

A complementary approach to finding nearby substellar objects is to use proper motion measurements. A local disc star with a transverse velocity of $V_T = 20\,km\,s^{-1}$ relative to the local standard of rest and a distance of $d = 50\,pc$ has a proper motion of $\mu \simeq 80\,mas\,yr^{-1}$. Given the 5 yr baseline of the DES survey, the resulting displacement of 0.4 arcsec is expected to be measurable with the DES data. DES obtains about 15 mas relative astrometric accuracy per exposure for bright objects, limited by atmospheric distortions.

The large number of L and T dwarf candidates will provide excellent targets for spectroscopic follow-up, which may help to constrain atmospheric models of these objects. We note that the Chabrier et al. (2000) models used in the simulations by Rossetto et al. (2011) typically have colours which are systematically blue compared to those observed in Sloan Digital Sky Survey (SDSS; Knapp et al. 2004; Day-Jones et al. 2013b), even after differences in transmission between DES and SDSS filters are taken into account. More recent models from Saumon & Marley (2008) display redder colours by ≃0.2 mag, but still have trouble reproducing the observed colour locus for later-type objects.

4.2 Luminosity function of thick disc and halo M dwarfs

Over 70 per cent of the stars observed by DES will belong to the thick disc and halo of the Milky Way. Low-mass MS stars with $0.08 < M/M_\odot < 0.50$ will dominate the DES stellar sample. About 7.5×10^7 red dwarfs are expected to be imaged (Rossetto et al. 2011). Even in the presence of significant sample incompleteness and galaxy contamination, the number of stars in the typical colour range of M dwarfs will constrain the slope of the stellar IMF, $d\log N(m)/d\log(m)$, for these Galactic components to a precision of better than 0.1 dex.

The relatively straightforward colour selection for low-mass stars coupled with the large survey footprint of DES will allow us to study the structure of the Galactic disc with unprecedented detail. In particular, we will be able to detect new stellar substructures close to the Galactic plane and to search for asymmetries with respect to the Northern hemisphere (comparing to similar star counts from SDSS, for instance; Jurić et al. 2008).

4.3 The luminosity function of thick disc and halo white dwarfs

White dwarfs (WDs) are the end point of stellar evolution for the majority of stars. The faint end of the WD luminosity function (WDLF) is occupied by the oldest members of a given stellar population, those that are the furthest along the WD cooling sequence. Therefore, the WDLF of the disc and the halo provides a method of dating the early star formation in each of these Galactic components (Althaus et al. 2010). Additionally, modelling of the WDLF can be used to constrain the stellar IMF and SFH (van Oirschot et al.

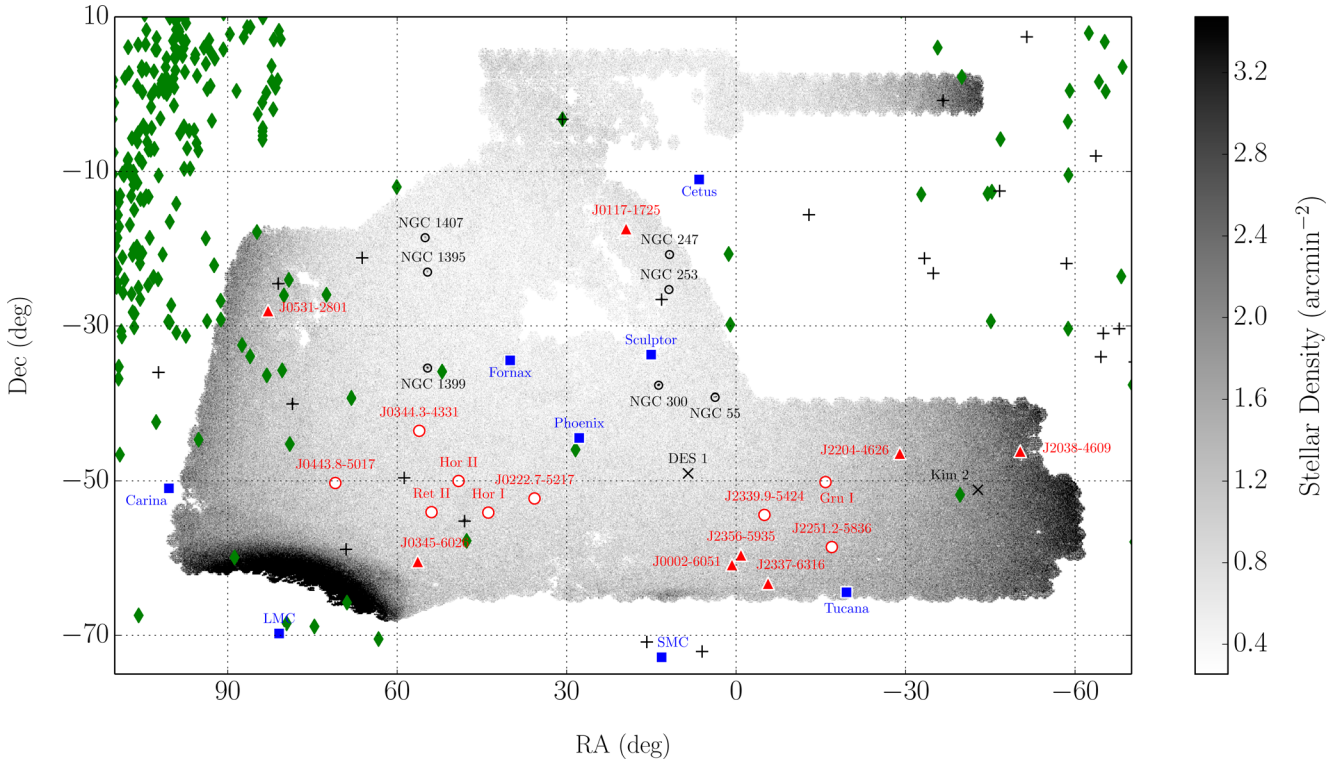

Figure 6. Cartesian projection of the density of stars observed in both g and r bands with $g < 23$ and $g - r < 1$ over the DES Y2Q1 footprint ($\sim 5000\,\mathrm{deg}^2$). Globular clusters are marked with '+' symbols Harris (1996, 2010 edition), two faint outer halo clusters are marked with '×' symbols (Luque et al. 2016), Local Group galaxies known prior to DES are marked with blue squares (McConnachie 2012), dwarf galaxy candidates discovered in Y1 DES data are marked with red outlined circles, while the Y2 stellar systems are marked with red triangles. Open clusters from the WEBDA data base are shown as green diamonds. The periphery of the LMC can be seen in the south-east corner of the footprint, while the Galactic stellar disc can be seen on the eastern and western edges. This figure was adapted from Drlica-Wagner et al. (2015b).

2014). WDs are also an important class of objects for photometric calibration. Both DES and other future large-area surveys will benefit from the discovery and characterization of WDs in the DES footprint.

The search for nearby WDs will benefit greatly from the availability of proper motions. Since DES will not measure u-band magnitudes, WD samples selected by $(g - r)$ colour will be contaminated by A and F stars from the Galactic disc and halo main-sequence turn-off (MSTO). The DES Y-band images may be useful due to the signature of strong Paschen absorption lines in the spectra of DA WDs. An excess of objects relative to model predictions for MS stars of similar colours may also be used to constrain statistically the WDLF.

Unfortunately, MS contamination is aggravated for WDs close to the end of the cooling sequence, which are the most useful to determine the down-turn of the WDLF and estimate the age of each Galactic component. For this population, proper motion measurements will be crucial to separate kinematically a local WD population from more distant MS stars of similar colours.

4.4 Membership and luminosity functions of galactic open clusters

Galactic open clusters are unique astrophysical laboratories for understanding stellar evolution. Their ages can be fairly accurately determined by isochrone fitting of cluster colour–magnitude diagrams (CMDs; e.g. Cargile & James 2010), by determining the lithium burning-limit age (e.g. Basri, Marcy & Graham 1996; Cargile, James & Jeffries 2010) or by populating rotation-period versus photometric colour space (gyrochronology; Barnes 2003, 2007; James et al. 2010). In Fig. 6, we plot the positions of open clusters from the extensive, although surely incomplete, WEBDA open cluster data base (circa February 2015).[13] We also plot the positions of globular clusters and Local Group dwarf galaxies, which will be discussed in Sections 4.8 and 4.10, respectively. 17 of these open clusters are located in the DES footprint. Only 3 of these 17 clusters have well-determined physical properties, tending to be relatively nearby ($\ll$1 kpc), young ($\ll$4 Gyr), and either thin- or thick-disc ($z < 500$ pc) systems. The well-studied Blanco 1 open cluster lies on the boundary of the footprint, and was surveyed in *griz* during SV (to a 5σ limiting magnitude of $g \simeq 22$).

It is relatively straightforward to establish membership using colour–magnitude and colour–colour diagrams for an exemplar open cluster, such as the rich, nearby (120 pc) and young (125 Myr) Pleiades (Stauffer, Schultz & Kirkpatrick 1998; Robichon et al. 1999). However, based on SV data, all higher mass stars (earlier than G0V) are saturated in low-extinction DES fields out to 3 kpc (which if perpendicular to the Galactic plane is about three times the thick-disc scaleheight). At that distance (neglecting interstellar extinction), all cluster G, K and M dwarfs are detected (S/N > 10), whereas all substellar objects (brown dwarfs) and degenerate compact objects (WDs) are far below the detection threshold (see also Table 2; Rossetto et al. 2011).

[13] http://www.univie.ac.at/webda/navigation.html

For a closer cluster located at ~ 1 kpc (about three times the thin-disc, and one thick-disc, scaleheights), only K- and M-dwarf stellar members are non-saturated, although the entire brown-dwarf population will still fall below the survey's magnitude limit. Of the 17 open clusters in the DES footprint, 3 have well-determined distances and are closer than 300 pc. For these systems, DES survey detections will only be possible by using their early-mid L-dwarfs and some post-Luminosity Function peak WDs (depending on cooling age).

In all likelihood, the primary utility of multifilter photometry of open clusters in the DES footprint will centre on defining the number, space density and photometric properties of very red low-mass stars and high-mass brown dwarfs. By constructing cluster mass functions at the stellar/substellar boundary, we will directly complement Galactic field IMF studies for late-M, L- and T-dwarfs. A side-by-side comparison of Galactic field and open cluster IMFs provides an empirical test for the magnitude and time-scale of mass segregation and cluster disruption/evaporation (e.g. Moraux, Kroupa & Bouvier 2004). Further science goals arising from DES open cluster observations could include (a) detection and characterization of the WD sequence for the closest clusters, allowing an age derivation from theoretical cooling sequences to be calculated and compared to traditional age determination methods (e.g. Kalirai et al. 2001) and (b) sensitivity to magnetic activity-induced stellar variability for the most distant clusters. While the wide-field DES survey will possess too few epochs for precise determinations of rotational periods, cluster members will be able to be identified from their photometric variability (e.g. James et al. 2010).

4.5 The shape of the galactic stellar halo

There are discrepant estimates of the axial ratio (and its variation with Galactocentric distance) for oblate models of the Galactic stellar halo (Du et al. 2008; Jurić et al. 2008; de Jong et al. 2010). Using the integrated numbers of stars in the typical colour range of old low-metallicity F and G stars, Rossetto et al. (2011) show that the axial ratio of the stellar halo can be constrained to within 1–2 per cent, again assuming efficient star–galaxy separation. More interesting is the prospect of exploring other halo geometries, including effects of triaxiality and asymmetries. The task of constraining these more complex models will greatly benefit from defining a joint DES/SDSS stellar sample.

4.6 Detection and characterization of variable stars

In addition to a large spatial footprint, DES will span a 5 yr temporal period. Each of the wide-field pointings will be observed 10 times in each band over the duration of the survey. At the same time, each of the 10 DES-SN fields (covering a total of 27 sq deg) will be observed regularly with a 7 d cadence. This large multi-epoch data set presents an exciting opportunity for discovering temporally variable stars.

Even the limited number of observations available in the wide-field survey should be sufficient to discover new pulsating variable stars. One straightforward method for identifying variable stars is to compare the flux measured in each epoch to the median flux of the object. Preliminary searches for δ-Scuti and RR Lyrae stars in the SDSS Stripe-82 region show that this type of selection can yield a variable star completeness of $\geq$70 per cent with a purity of $\geq$50 per cent. The completeness and purity of this technique is significantly enhanced in the SN fields where the number of observations is much larger. Additional calibration is possible using the known populations of variable stars in the Large Magellanic Cloud (LMC) and the Reticulum globular cluster (Section 4.8).

4.7 Detection and characterization of galactic stellar streams

Stellar streams often span tens of degrees on the sky; they originate from tidal stripping of stars from globular clusters and dwarf galaxies. Models of cold stellar streams yield constraints on the total mass distribution and on the number of DM subhaloes orbiting the Galaxy (Yoon, Johnston & Hogg 2011), and also allow the inference of Galactic parameters and of the properties of the progenitor system (Koposov, Rix & Hogg 2010; Küpper et al. 2015).

Several known tidal streams, including one associated with the Sagittarius dwarf galaxy, are expected to extend into the DES footprint. Often, these halo substructures are found by inspecting the spatial distribution of halo tracers, such as horizontal branch, red giant or halo MSTO stars (e.g. Yanny et al. 2000; Belokurov et al. 2006). Indeed, one new stream has been discovered in the Y1 data (Balbinot et al. 2016). Another stellar stream associated with the LMC has been identified by Mackey et al. (2016).

DES will also be sensitive to low-density extra-tidal features around globular clusters. A tool for identifying tidal features has been developed within the DES Collaboration and applied to NGC 2298, a relatively low latitude globular cluster (Balbinot et al. 2011). This tool applies a matched-filter algorithm to measure the density of stars associated with a known cluster across the field.

4.8 Local Group globular clusters

Local Group globular clusters provide a rich population of resolved objects for study with DES. These objects trace some of the oldest and most nearby stellar populations. They allow us to probe the gravitational potential of the Local Group both through the bulk orbital motion and through the tidal disruption of their member stars (as discussed in Section 4.7). Additionally, the dense resolved stellar populations of globular clusters provide a test bed for star–galaxy classification, determinations of proper motion and precision astrometric calibrations. Globular clusters can also be used to calibrate a photometric metallicity scale for DES filters in the range of $-2.1 \leq [\mathrm{Fe/H}] \leq -1.2$.[14] Two globular clusters of particular interest to the DES survey are Omega Centauri and Reticulum.

Omega Centauri is a dense Milky Way globular cluster located at (RA, Dec.) = ($13^{\mathrm{h}}27^{\mathrm{m}}$, $-47^{\circ}29'$). The retrograde orbit of Omega Centauri suggests that this globular cluster may have originated as a dwarf galaxy and was tidally stripped by the Milky Way (Carraro & Lia 2000). Recent searches for tidal tails of Omega Centauri show no current tidal disruption (Da Costa & Coleman 2008); however, the wide coverage of DES and its depth at red wavelengths should provide unprecedented sensitivity to tidal features in the old stellar population of Omega Centauri. In addition, the relative proximity and high stellar density of Omega Centauri make it an excellent candidate for studying stellar proper motion.

The Reticulum globular cluster, located at (RA, Dec.) = ($04^{\mathrm{h}}36^{\mathrm{m}}$, $-58^{\circ}52'$), resides within the SV SPT-E field. Reticulum is at a distance comparable to that of the LMC and is likely gravitationally bound to that galaxy (Walker 1992; Dall'Ora et al. 2004; Sollima et al. 2008). Its age and metallicity have been determined using

[14] Complementing DES with u-band data will be important for this task, since CN and NH features affect the u filter (e.g. Ivezić et al. 2008; Marino et al. 2008; Carretta et al. 2009).

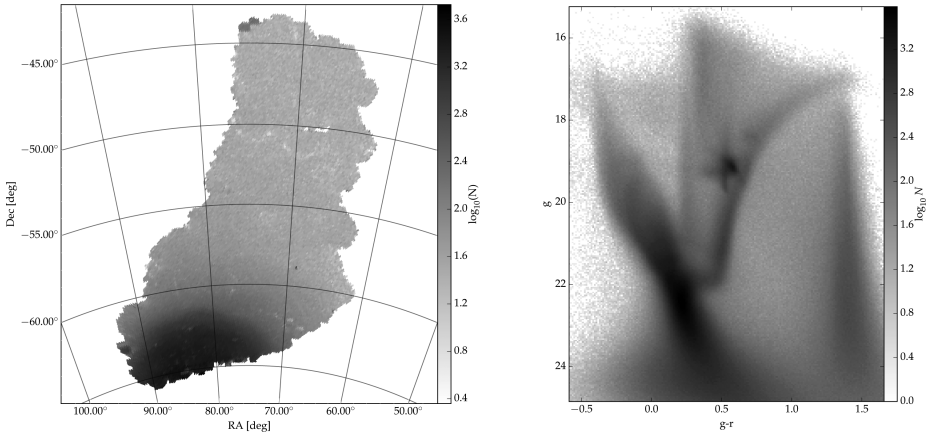

Figure 7. Left: density map of sources classified as stars in the SPT-E region covered by the DES SV data; Right: g versus $(g - r)$ Hess diagram of all objects classified as stars and located at Dec. $< -55°$. The LMC MS stars are visible over almost the entire magnitude range. More than one MSTO point is present, attesting a large age range which includes an old population with MSTO at $(g, g - r) \simeq 22.5, 0.3$. Clear subgiant and red giant branches (SGB and RGB, respectively) associated with the older populations are also seen redwards of $(g - r) \simeq 0.4$ for $g < 22.3$. The width both at the MS and at the RGB attest a significant metallicity spread as well. The red clump and horizontal branches are also clearly visible. The AGB bump is also visible at $g = 18.5$ and $g - r = 0.7$.

HST-ACS (*Hubble Space Telescope*) data by Mackey & Gilmore (2004) and are typical of the LMC old cluster population. The DES coverage around this cluster will allow the detection of extra-tidal features associated with this system, which in turn will help constrain the gravitational potential in the outer regions of the LMC. The combination of spatial coverage and photometric depth will allow a more thorough investigation of the cluster's structure, with improved determinations of its current mass function, mass segregation and binary fraction. These characteristics will allow us to diagnose the role played by internal dynamical effects.

The Reticulum cluster serves as a distance reference, since it is known to be associated with the LMC and to contain many RR Lyrae stars (Kuehn et al. 2013). The wide-area coverage of the SPT-E data will help increase the census of these objects, specifically in the cluster outskirts.

Besides the two exemplars discussed above, Harris (1996, 2010edition) lists eight additional Milky Way globular clusters that are covered by DES and several other globular clusters that lie close enough to the survey border to allow for searches for extra-tidal features (Fig. 6).

4.9 Stellar structure at the outskirts of the LMC

The largest contiguous area of the DES SV data is the SPT-E. The SPT-E field covers a region roughly 8° on a side in the declination range $-64° \leq$ Dec. $\leq -46°$. The southern border of the SPT-E region is located $\simeq 4°$ from the centre of the LMC. Therefore, SPT-E provides a uniform and deep sample of LMC stars ranging from 5 to 22 kpc in projected distance from the LMC centre. The left-hand panel of Fig. 7 shows the number density of stellar objects in the SPT-E field, where one can clearly see the steep rise in stellar density. The right-hand panel shows a CMD of a region 0.5 sq deg located $\simeq 6°$ from the LMC centre (RA, Dec.) = (78°06′, −63°54′). This region is clearly dominated by LMC stars spanning a wide range of ages and metallicities. The complex structure of He burning stars in the red clump and horizontal branch is clearly visible, including the secondary clump stretching vertically from the blue end of the main red clump (Girardi 1999).

The contiguous coverage of the SPT-E field has already allowed us to constrain the structure and density distribution of the LMC disc out to $\simeq 20$ kpc. Balbinot et al. (2015) have fitted the LMC star counts to a disc model and found it to have an inclination $i = 38.^{\circ}7$ relative to the plane of the sky with a position angle of $\theta_0 = 129°$ and an exponential scale radius $R_s = 1.11$ kpc. A significant variation in this latter parameter has been observed as a function of age: $\tau \leq 2$ Gyr stars have $R_s = 0.7$ kpc, whereas older stars are spread over twice this value along the LMC disc plane. The authors have also found this disc to be warped and likely flared in the outermost LMC regions probed. These results confirm, out to larger LMC radii, previously observed age and metallicity gradients with older and more metal poor stars located in the outer regions (Carrera et al. 2008; Gallart et al. 2008).

The existence of a spherical stellar halo associated with the LMC remains an open question (Gallart et al. 2004; Carrera et al. 2011). Determining the extent out to which LMC stars are to be found and whether this galaxy has its own system of satellite galaxies and other substructure also requires a large coverage in area and depth. Data from DES and from the Survey of the Magellanic Stellar History (SMASH; Martin et al. 2015), when jointly analysed, should provide a much more detailed picture of the stellar content of the LMC, the Small Magellanic Cloud (SMC) and the entire Magellanic system. These data will be sensitive to spatially varying SFH of LMC stars using the available CMDs at different directions across the field. Mapping the SFH of the LMC at large distances will allow a more detailed assessment of the radial extent of the observed age and abundance gradients, which suggest an outside-in galaxy formation history.

A more complete census of RR Lyrae stars belonging to the LMC and SMC is expected to result from these data, especially in its outermost regions. This will, in turn, provide an independent assessment of the structure and geometry of the external components of these galaxies (Kinman et al. 1991). Finally, new star clusters and stellar substructure associated with LMC have been identified and characterized with SV data (Pieres et al. 2015).

4.10 Detection and characterization of Milky Way satellite galaxies

Hargis, Willman & Peter (2014) predict that 3 to 13 new dwarf galaxies with $L > 10^3\,L_{\odot}$ should be found by DES and a factor of a

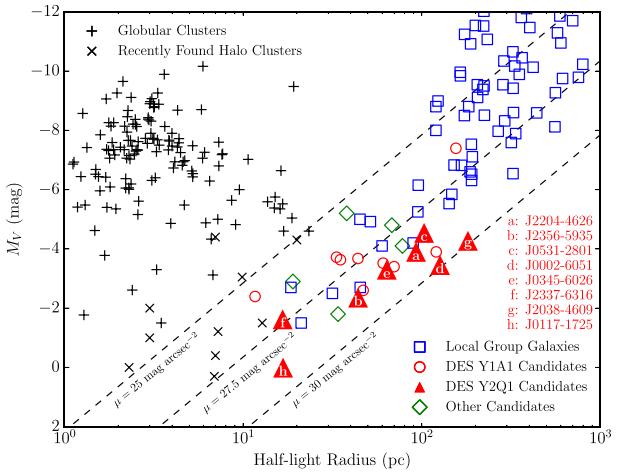

Figure 8. Absolute *V*-band magnitudes and half-light radii of MW satellites and Local Group dwarf galaxies. MW globular clusters are marked with '+', fainter clusters and ambiguous objects are marked with '×', while spectroscopically confirmed dwarf galaxies are marked in blue. The red markers show the new dwarf galaxy candidates found in DES Y1+Y2, while green markers show candidates found in other surveys. Figure taken from Drlica-Wagner et al. (2015a).

few as many below this luminosity. On the other hand, Tollerud et al. (2008) estimate that 19 to 37 new Milky Way satellites could be discovered by DES, assuming that the detectability of these satellites is similar to those discovered in SDSS (Koposov et al. 2008; Walsh et al. 2009), but extending to the deeper limiting magnitude of DES. However, Rossetto et al. (2011) used an analytical model for the stellar IMF and the mass–luminosity relation of MS stars to show that the number density contrast of satellite stars relative to the background may increase by as much as 70 per cent in the DES sample when compared to SDSS. Since DES will reach the MS of old stellar populations out to $\simeq$120 kpc, it will be sensitive to stellar systems at larger distances than SDSS. The DES Collaboration has developed a suite of tools, including matched-filter and maximum-likelihood algorithms, to search for Milky Way satellites in the DES footprint.

Analysis of Y1 DES data has already revealed nine new MW satellite galaxy candidates that have sizes and luminosities consistent with ultra-faint dSph galaxies (Bechtol et al. 2015; Kim & Jerjen 2015; Koposov et al. 2015a). Analysis of Y2 data added eight more systems to this tally (Drlica-Wagner et al. 2015b). In Fig. 8, we compare the newly found objects (red markers) to star clusters and other dwarf galaxies from the Local Group.

Since dwarf galaxies are very DM rich, they are potential astrophysical targets for the indirect detection and characterization of DM particles through annihilation into high-energy photons (Bringmann & Weniger 2012). Analysing gamma-ray data coincident with the newly discovered dwarf galaxy candidates has been the subject of much recent interest (Drlica-Wagner et al. 2015a; Geringer-Sameth et al. 2015; Hooper & Linden 2015). Meanwhile, better estimates of the DM content of the new systems are being actively pursued via spectroscopic observations (Koposov et al. 2015b; Simon et al. 2015; Walker et al. 2015). Gamma-ray observations of new faint dwarf galaxies are expected to be sensitive to the generic prediction for an annihilation signal from one of the prime DM candidates, the weakly interacting massive particle.

DES will also cover several classical Milky Way satellites and Local Group dwarf galaxies, including Fornax, Phoenix, Sculptor and Tucana. The deep, wide and homogeneous coverage provided by DES will allow the spatial stellar distribution of these systems to be probed beyond their tidal radii, therefore improving their mass estimates and helping constrain the mass of the MW halo out to their location.

5 SEARCH FOR OPTICAL COUNTERPARTS OF GW EVENTS

The GW ground-based interferometric detectors, LIGO and Virgo, anticipate first detections within this decade (LIGO Scientific Collaboration 2013). Detectable GW events are expected from mergers of neutron star (or black hole) binaries out to about 200 Mpc. Such mergers are also expected to produce a fast, red, faint transient that optical telescopes might detect (Abadie et al. 2010; Aasi et al. 2014). This poses a unique opportunity to perform the first detection of gravitational and electromagnetic radiation from the same astrophysical sources and, therefore, to learn more about the astrophysics of neutron stars, the nucleosynthesis of heavy elements in the Universe and its recent expansion history. The DES Gravitational Waves (DESGW) project aims to search for the optical counterparts of the first LIGO–Virgo detections using DECam. The main challenge is to cover the large regions where the source might be located: GW detectors have large uncertainties on the sky localization of a source (typically 300 sq deg in the late 2015–early 2016 observing run, expected to improve by a factor of a few in the next run). Fortunately, DES is well equipped to meet this challenge, with a 3 sq deg field of view camera mounted on a 4 m telescope.

The DESGW programme has been granted three additional nights of DECam time in 2015B semester to perform the first search campaign and we expect to expand this programme in future years. The three nights of the DESGW programme are merged with the regular DES time allocation. When an event follow-up is to occur, we modify the observing plan for that night to perform observations covering the event's region of interest and subtract the time used from our three-night allocation.

We have developed a system that watches for alerts from the GW detection consortium. Once an event trigger happens, the system processes the GW probability maps to determine the optimal observing plan for that particular event and estimates the probability of detection of the hypothesized optical counterpart. Fig. 9 shows an example of a simulated GW event at a distance of about 119 Mpc. For this particular example, we assume that the absolute magnitude of the optical counterpart is $M = -11$ in the i band and that the light curve decays in about 10 d. These parameters are chosen to match the sensitivity range of the LIGO detectors in the late 2015–early 2016 run and the baseline emission model (merger of a pair of neutron stars with 1.4 solar masses each).

For each event, we produce a plan for observations to be made within 24 h from the trigger time. The probability of detection takes into account the source model, the distance, the depth achievable for that night (accounting for sky brightness, Galactic extinction and exposure times). We plan observations in i and z bands to make use of colour information. For the particular event shown in Fig. 9, we expect to reach 49 per cent detection probability in 44 hexagon(s) (each hex corresponds to the area of 1 camera field, which covers 3 square degrees). This is a typical event. About 25 per cent of the simulations have total detection probability at this level or better.

To perform these searches, we need to do difference imaging. DES does difference imaging routinely in 10 dedicated fields, the

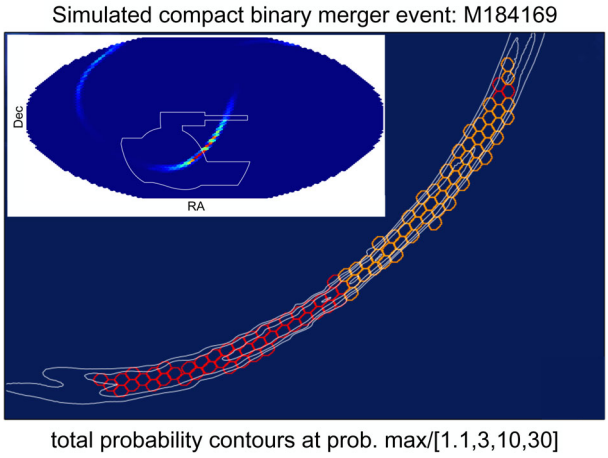

Figure 9. Example of a simulated GW event trigger provided by the LIGO–Virgo Collaboration (LVC). Such simulations are used to optimize observing strategies and estimate detection probabilities. The event M184169 shown in this example is at 119 Mpc distance and the LVC probability map shows the probability of the event falling in a given sky pixel. The inset shows the full-sky probability distribution derived from the GW data, with the larger figure showing the area that would be observed by DECam on the first night after the trigger The red hexagon(s) are inside the DES footprint, and the orange ones are outside. The white contours represent the total LVC probability density times detection probability, assuming a source of absolute magnitude $M = -11$ at the trigger distance.

SN fields. We generalized the SN difference-imaging pipeline to work on any area of the sky using any available DECam image. This work will benefit other transient searches in DES (e.g. Solar system, NEOs, nearby SNe and quasars).

The start of operations of the LIGO–Virgo network of advanced GW detectors combined with observations of their optical counterpart will potentially enable ground-breaking results, including the first detection of mergers of black holes and neutron stars, study of the evolution of binary systems, measurements of the equation of state of neutron stars, determination of the origin of r-process elements in the Universe and a novel cosmological probe. In the long run, we expect that GW events will be used to measure the distance–redshift relation with great precision (Schutz 1986; Holz & Hughes 2005). A sample of 20–30 well-measured events can result in measurement of the Hubble parameter with uncertainty of 3 per cent. Future experiments may provide tens of thousands of such events. The DESGW programme will capitalize on the ground-breaking potential of combined GWs and optical observations. Simultaneous detection of GW and photons can also provide measurements of the speed of gravity and test modified theories of gravity (Desai, Kahya & Woodard 2008; Nishizawa & Nakamura 2014).

In 2016 February, the LIGO Collaboration reported the first detection of gravitational waves, GW150914, resulting from the merger of two black holes (LIGO Scientific Collaboration & Virgo Collaboration 2016). DES provided optical follow-up of this event, as described in Abbott et al. (2016), Annis et al. (2016) and Soares-Santos et al. (2016). No optical detections were detected, which is not surprising, as in the conventional model a binary black hole merger is not expected to have any optical counterparts, and the DES observations covered only part of the sky where the event was likely to happen. However, DECam will be vital for future LIGO follow-ups.

6 GALAXY EVOLUTION

The DES data set, though designed for DE studies, presents a gold mine for galaxy evolution science. The science covered is very broad and includes studies of galaxies and galaxy properties across redshift space from the nearby universe to epochs close to reionization around $z \sim 6$. This will be possible thanks to the unprecedented combination of wavelength coverage, width and depth of DES+VHS photometry. Here we describe some of the broad science themes enabled by the DES data: (1) the evolution of the multivariate and stellar population properties of galaxies and their evolution with redshift, (2) galaxy environment, (3) galaxy luminosity and mass functions and their evolution with redshift, (4) massive galaxies at high redshift, (5) connecting galaxies to their DM context, (6) galaxy properties in galaxy clusters and (7) intracluster light (ICL). A major shortcoming in traditional galaxy surveys designed for galaxy evolution studies is the lack of sufficient volume required to overcome limitations caused by both cosmic variance and the low number density of massive galaxies. Thanks to the large survey area of 5000 sq deg, the volume sampled in DES is orders of magnitude larger than existing galaxy evolution surveys, at the price of being shallower by several magnitudes. With this unique combination of intermediate depth and large volume, the DES data set will allow a major step forward in the field. In the following, we briefly discuss the key topics that we envisage being addressed by DES.

6.1 Stellar population properties

The relatively wide wavelength range covered by the DES photometry allows far more than just the derivation of photometric redshifts, in particular when the VHS near-IR data are included. The moderate depth even in the reddest bands with $z \sim 23$ mag (AB) and $Y \sim 22$ mag will be used for the analysis of the galaxy population for a relatively large luminosity range up to redshifts $z \sim 1$. This particular epoch, at which the Universe had about half of its current age, is critical for understanding galaxy formation and evolution. It represents the time of transition in the evolution of galaxies, where, viewed as a function of increasing redshift, a largely passively evolving population is believed to have broken up into its hierarchical pieces (e.g. De Lucia & Blaizot 2007). The photometric bands g to K cover the rest-frame wavelength range $2200 < \lambda < 10\,000$ Å around those redshifts, hence providing a good sampling of the SED. Stellar population model fits will provide key galaxy parameters such as stellar population age, SFH, star formation rate, metallicity, dust attenuation, slope of the IMF, absolute luminosity and stellar mass (e.g. Bolzonella et al. 2010; Maraston et al. 2010). Redshift evolution will help to break well-known degeneracies between some of these parameters. The power of the DES data to study galaxy evolution will largely lie in its ability to describe the joint distribution of a wide range of galaxy properties, thereby determining correlations between galaxy properties and the environment, and how these correlations evolve with redshift. The joint distribution of several of these properties is now well studied in the local universe from the SDSS (e.g. Blanton & Moustakas 2009; Thomas, Abdalla & Lahav 2011). DES will allow extensions of these studies to $z \sim 1$ with a fine enough binning to separate the various correlations to a degree that is not possible with smaller surveys.

6.2 Galaxy environment

Thanks to the large volume sampled by DES, the data set will allow the investigation of galaxy environment beyond the local universe

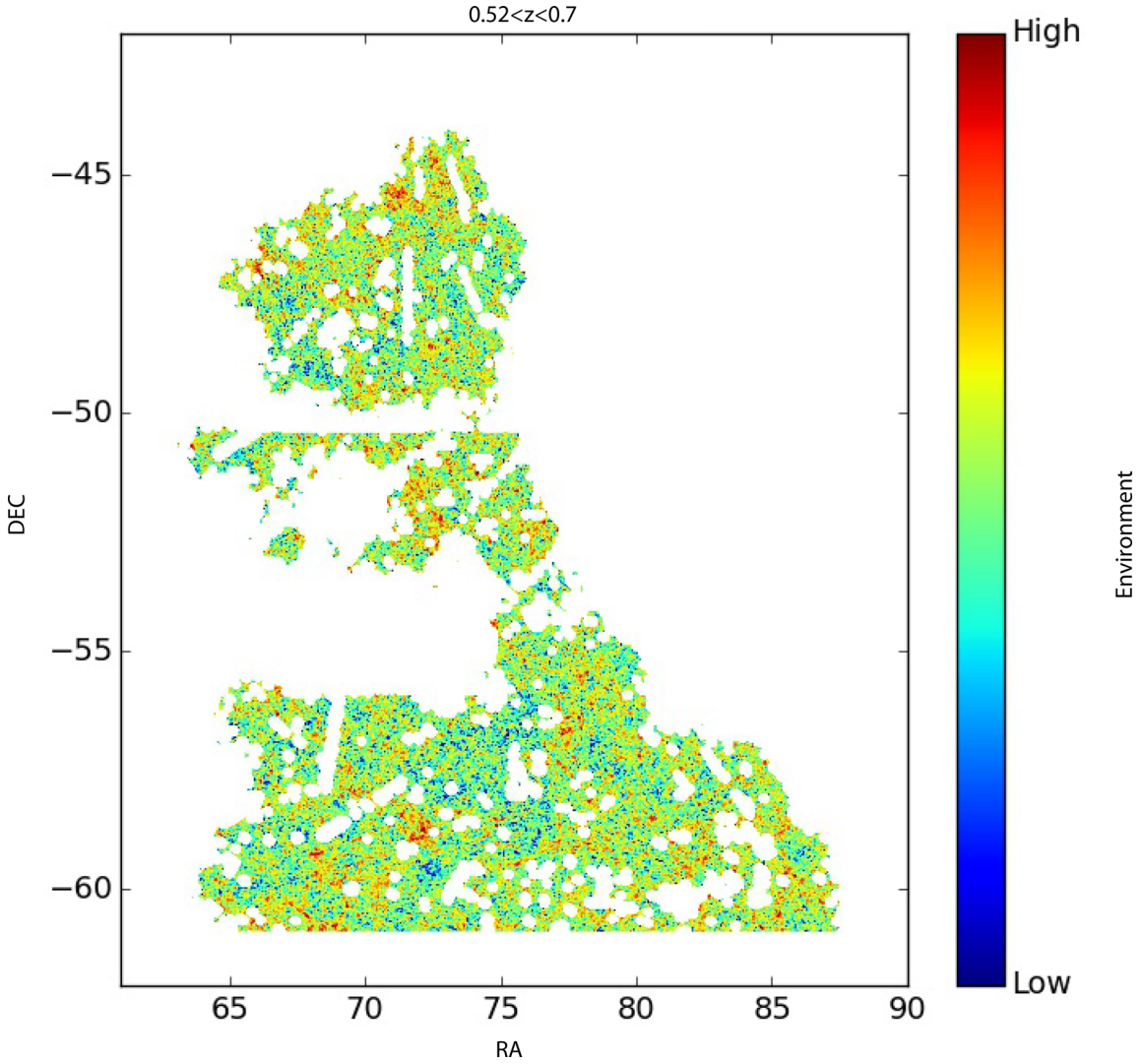

Figure 10. Galaxy environment maps derived from photometric redshifts in a slice at redshift $0.52 < z < 0.70$ for a ≈100 sq deg footprint overlapping with the SPT-E field derived from the DES SV data. Dense environments are shown in red and sparse environments in blue.

up to $z \sim 1$. This large sample comes at the cost of redshift precision, and this affects environmental measurements. Spectroscopic redshifts have been key in studies of environmental effects in the local universe (Peng et al. 2010; Thomas et al. 2011; Brough et al. 2013) and at higher redshifts (DEEP2, COSMOS); by contrast only photometric redshifts are available in DES.

In preparation for the DES, Etherington & Thomas (2015) investigated the impact of the photometric redshift precision on measures of galaxy environment. They studied this by measuring environments using SDSS spectroscopic and photometric redshifts; they also simulated photometric redshifts with a range of uncertainties. Photometric measurements have a smaller dynamic range than spectroscopic measurements because uncertain redshifts scatter galaxies from dense environments into less dense environments. At the expected redshift uncertainty of DES of $\sigma_z = 0.1$, they found a Spearman's rank correlation coefficient of 0.4 between the photometric and spectroscopic measurements.

They further showed that the bivariate dependence of the galaxy red fraction on stellar mass and environment (e.g. Peng et al. 2010) can be reproduced using photometric redshifts. They concluded that photometric samples with a redshift uncertainty of 0.1 must be approximately 6–16 times larger than spectroscopic samples to detect environment correlations with equivalent fractional errors. This requirement is easily met by DES. Fig. 10 maps environmental densities calculated from a subset of the SPT-E field in the DES SV data using the full probability distributions of photometric redshifts provided by the TPZ code (Carrasco Kind & Brunner 2013, 2014).

6.3 Luminosity and stellar mass functions of galaxies

How the massive ($\gtrsim 10^{11}$ $M_\odot$) end of the stellar mass function builds up over cosmic time is still a matter of debate. If constructed using hierarchical structure build-up, then this part of the mass function evolved significantly in the last ∼10 Gyr, during which time galaxies accreted between 20 and 50 per cent of their final mass. Observations, however, hint at a mass-dependent galaxy number density evolution with redshift, i.e. the larger the mass, the milder the number density evolution (Cimatti 2006; Marchesini et al. 2009; Pozzetti et al. 2010). These discrepancies between observations and theoretical models lead to uncertainties regarding galaxy formation. These uncertainties could be reduced by having a survey with a volume large enough to detect a representative sample of the most

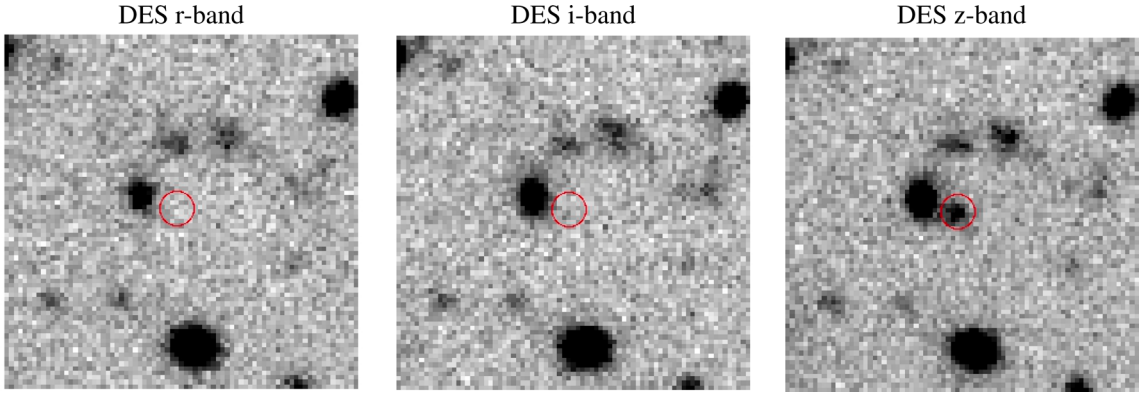

Figure 11. DES *r*-, *i*- and *z*-band images in the DES deep fields for a spectroscopically confirmed galaxy at $z = 6.07$ galaxy from Willott et al. (2013). The galaxy position is marked by the red circle in all three images. As can be seen, this high-redshift galaxy is undetected in the DES *r* and *i* bands but detected in the redder DES *z* band. This characteristic 'dropout' behaviour of high-redshift galaxies can be exploited to find similar $z > 6$ galaxies in the DES deep fields.

massive galaxies in the Universe (the rarest part of the galaxy population), and deep enough to identify a galaxy sample complete both out to a sufficiently low mass and out to $z \sim 1$.

More recently, the Baryonic Oscillation Spectroscopic Survey (Dawson et al. 2013) provided a data set that allowed the study of the number density evolution of massive galaxies up to $z \sim 0.7$. Based on these data, Maraston et al. (2013) showed that the massive end of the galaxy mass function has not been evolving since those redshifts (see also Bernardi et al. 2016). DES will allow us to extend this study both to higher redshifts and to lower mass galaxies covering key parameter space of the galaxy mass function. Thanks to the large data set further key parameters such as environmental density, galaxy type, colour, etc. can be folded in the analysis at high statistical significance.

6.4 Galaxies at high redshifts

The deep photometry and large volume probed by DES will further enable statistical studies of galaxies at $z \sim 3$–6, and especially of the massive end of the galaxy population where other surveys are limited by small sample size. The overlapping VISTA data will be very useful for these studies. The analysis of extended and statistically significant samples of red galaxies will be pushed up to $z \sim 6$, close to the epoch of reionization.

Galaxies at $z \sim 3$ are usually singled out as 'dropouts' (a.k.a. Lyman-break galaxies, LBGs) through successive passbands; this makes use of the strong Lyman-break signature in their SEDs (e.g. Steidel, Pettini & Hamilton 1995). The multiband data from DES will be sufficiently deep that they can be used to select galaxies from $z \sim 4$ to 6 in three redshift bins as *g*, *r*, *i*-dropouts. If young, massive galaxies have already assembled at high redshift, then DES will be able to detect them. This observation is exciting as the presence of such objects is expected from the fossil record of local massive galaxies (Thomas et al. 2011), but could not be easily accommodated in theories of hierarchical galaxy formation based on cold dark matter cosmogonies (e.g. Baugh et al. 2005). Davis et al. (2013) investigate the potential for DES to detect such objects in a study based on stellar population modelling and the DES simulated data. They show that very young massive galaxies would be found, if they exist and are not heavily dust obscured. The combination of sky coverage and photometric depth of DES is the key. Narrow, deep surveys, usually designed for the detection of high-*z* galaxies (Stanway, Bunker & McMahon 2003; Bouwens et al. 2010), do not cover enough volume to find rare massive galaxies. DES will play a unique role in this field as its 5000 sq deg survey area will enable us to set a stringent constraint on the brightest end of the galaxy luminosity function between $z \sim 4$ and 6. Precise knowledge of the bright end behaviour of the luminosity function will have an enormous impact on a series of critical cosmological questions, such as the star formation process at very early epochs and the reionization of the Universe.

In addition to the searches for massive high-redshift galaxies in the DES wide survey, the DES deep SN fields will also be a gold mine for studying the high-redshift universe and the epoch of reionization. One of the most fundamental questions in galaxy formation research today is understanding when massive galaxies were first formed and quenched. Thousands of high-redshift galaxies at $z \gtrsim 6$ are now being routinely discovered using *HST* (e.g. McLure et al. 2011; Bouwens et al. 2015), but the bright end of the galaxy luminosity function at these redshifts can only be constrained using ground-based surveys over much wider fields. Recently, Bowler et al. (2014) have shown that the $z \sim 7$ luminosity function follows the DM halo mass function, which could mean that quenching mechanisms such as active galactic nucleus (AGN) feedback are yet to come into effect at these early epochs. Therefore, $z \sim 5$–6 represents a very interesting redshift range where the effects of mass related quenching first begin to be seen in the galaxy population.

The DES deep fields will reach 10σ co-add depths of ∼25–26 over ∼27 sq deg (Bernstein et al. 2012) enabling new samples of luminous $z \sim 5$–6 (LBGs) to be discovered. Fig. 11 shows a spectroscopically confirmed $z = 6.07$ galaxy (Willott et al. 2013) in the DES Y1 data. As can be seen, the galaxy is robustly detected in the DES *z* band but undetected in the *r* and *i* bands. This highlights that the DES Y1 data are already sensitive enough to detect $z \sim 6$ galaxies and the characteristic 'dropout' behaviour of high-redshift galaxies illustrated in Fig. 11 will be exploited to identify new high-redshift galaxies in the survey data. The DES deep fields also overlap with deep infrared surveys using VISTA (Jarvis et al. 2013) and *Spitzer* (Mauduit et al. 2012). Combining the optical DES data with these infrared data sets will also enable constraints on the stellar masses and SEDs of $z \sim 5$–6 galaxies.

6.5 Galaxy structure and morphology

One of the primary ways in which galaxies are studied is through the analysis of their structures and morphologies. The gross overall morphology of a galaxy (spiral, elliptical, peculiar) gives an indication of its formation state. Furthermore quantitative measures of

structure allow us to determine the distribution of light in galaxies, including how concentrated its light is, and whether or not a recent dynamical or star formation event has occurred. This is an area where DES will advance our knowledge considerably, given the higher resolution and depth of the data in comparison to previous surveys such as SDSS.

The type of measurements that DES will carry out include non-parametric and parametric fitting of galaxy structure. This includes measuring the concentration/asymmetry/clumpiness (CAS) parameters for the brighter sample of galaxies in DES (e.g. Conselice 2003), as well as using non-parametric fitting of surface brightness profiles to obtain effective radii, as well as Sérsic indices. These can be used together to trace the evolution in structure as a function of redshift, find galaxy mergers and quantify the structures of galaxies as a function of environment. A big mystery is why galaxies at a given mass become less concentrated and smaller at higher redshift (e.g. Buitrago et al. 2013), something that DES can address by examining how these features vary as a function of environment, SFH and halo mass. The overall morphologies can also be measured as part of Galaxy Zoo citizen science, whereby large members of the public can contribute to this aspect of DES.

The wide-field DES survey will image a total of nearly 2 million galaxies with stellar masses $M_* > 10^{10}$ M$_\odot$ at $z < 0.3$. This is significantly more than any other survey to date, and will allow us to determine how the morphologies and structures of massive galaxies vary as a function of other parameters such as stellar mass, environment and halo mass. We will also have some limited ability to trace the time evolution of galaxy structure. At increasing redshifts, a largely passively evolving population is believed to have broken up into its hierarchical pieces (e.g. De Lucia & Blaizot 2007), and the familiar Hubble-type morphologies give way to increasingly irregular-type galaxies (Mortlock et al. 2013).

DES will be able to trace the final stages of this process.

Within these measurements, statistical studies of the environmental dependence of galaxy properties, such as the so-called morphology–density relation, can be carried out as a function of redshift, and on a larger scale than has been possible before. There is a well-known correlation between galaxy structure and environment, such that early-type galaxies are more likely to be found in dense environments (e.g. Dressler 1980). With DES data we can go beyond simple morphologies and examine how the sizes and light concentrations of galaxies relate to environment and thereby tease out the effects of local and global densities on the structures of galaxies.

Furthermore, the DES data will allow us to study the faint galaxy population in the nearby universe for the first time, with several million galaxies fainter than $M_B = -17$ being resolved. This will give us the morphological properties of satellite galaxies, and allow us to determine the properties of dwarf systems which are found in void regions. This relates to recently discovered galactic conformity, whereby the central galaxies and their satellites have similar colours and SFHs (e.g. Hartley et al. 2015). DES will for the first time allow this conformity to be studied as a function of morphology and structure as well as the colour.

6.6 Evolution of galaxy properties in clusters

There has been much progress on characterizing the galaxy population in clusters at lower redshift ($z < 0.3$) with SDSS (Hansen et al. 2009), where excellent statistics have allowed selecting samples that share many common properties (e.g. by colour, position, and whether central or satellite) to isolate different contributions to galaxy evolution from typical physical processes in clusters such as ram pressure stripping, galaxy harassment and cluster tidal field interactions. Work with smaller volumes at higher redshift has demonstrated that some of the observed trends seem to be in place at $z \sim 1$ (Gerke et al. 2007), but the direct comparison of low- and high-redshift samples is hampered by the very different selection functions of the separate programmes. The rich and statistically significant sample of galaxies in clusters in DES data will enable such studies to push significantly further in redshift. Crucially, the DES data will provide not only a large sample of cluster members, but also a large sample of field galaxies with which to compare the cluster galaxies, allowing for a self-consistent measurement of the effect of cluster environment on galaxy evolution to $z \sim 1$. The DES data will enable greatly improved constraints on the galaxy population as a function of halo mass to high redshift, and, in comparison with large DES mock catalogues from high-resolution simulations, will be a key to unravelling the physics of galaxy transformation in cluster environments (Wetzel et al. 2013; Haines et al. 2015).

The brightest cluster galaxies (BCGs) in galaxy clusters tend to obey different relations between their mass, size and luminosity compared to satellite cluster galaxies (Bernardi et al. 2007; von der Linden et al. 2007). The properties of BCGs are closely coupled to host cluster mass (e.g. Hansen et al. 2009), as is expected from their privileged position near the centre of the DM potential well of galaxy clusters. Although the uniqueness of BCGs is often attributed to their likely distinct merger histories compared to more average galaxies (e.g. De Lucia & Blaizot 2007; Lidman et al. 2012), observational results remain inconclusive regarding which physical mechanisms are actually at work (Brough et al. 2008). DES's statistically significant sample of these rare objects will allow a systematic characterization of BCG properties as a function of host halo mass and redshift up to at least $z \sim 1$ (Zhang et al. 2016).

6.7 Measurement of the ICL

Galaxy clusters are found to contain a population of stars that are not bound to individual galaxies but which rather trace the cluster potential. The resulting diffuse ICL, which may contain 10–30 per cent of the total cluster light (Gonzalez, Zabludoff & Zaritsky 2005; Zibetti et al. 2005; Krick, Bernstein & Pimbblet 2006), is a fossil remnant of galaxy evolution in the cluster environment integrated over the course of a cluster's accretion history. The change in ICL as a function of redshift would provide valuable constraints on models of galaxy evolution in the cluster environment (Willman et al. 2004; Monaco et al. 2006; Conroy, Wechsler & Kravtsov 2007). While there has been detailed work to study a few tens of individual clusters at low redshift (e.g. Gonzalez et al. 2005; Krick et al. 2006; Pierini et al. 2008), constraints from these programmes remain weak owing to the small samples available. ICL measurements on stacked samples of clusters in the SDSS have been made (Zibetti et al. 2005), but uncertain systematic effects of such a technique make the interpretation of these results challenging. Based on current work using SDSS co-added southern stripe data to measure the ICL of individual clusters, it is expected that DES data, with careful control of data reduction tasks such as flat-fielding and sky subtraction, will enable the study of ICL in individual clusters to $z \sim 0.3$ over the full 5000 sq deg, an unprecedented volume for such work. Measurements from stacked clusters may be possible to even higher redshifts.

6.8 Galaxy biasing and halo modelling

The spatial distribution of galaxies does not necessarily follow the distribution of mass fluctuations. This is commonly referred to as 'galaxy biasing'; it could be linear/non-linear, deterministic/stochastic, local/non-local, and a function of scale and cosmic time. DES has the power to constrain biasing both on its own and in combination with other data sets. When deriving cosmological parameters from DES biasing appears as a set of 'nuisance' parameters, but if the cosmology is known (e.g. LCDM) or marginalized over, understanding biasing is important in its own right as a probe of galaxy formation and evolution (Benson et al. 2000; Gaztañaga & Scoccimarro 2005; Zehavi et al. 2011).

Galaxy biasing was recognized when it was noticed that different populations of galaxies have different clustering strengths (Davis & Geller 1976; Dressler 1980). A physical mechanism for galaxy biasing, namely that galaxies would tend to form in peaks in the matter density distribution thus being more clustered than the underlying matter distribution, was suggested by Kaiser (1984) and developed by Bardeen et al. (1986). In this picture, more massive (and thus rarer) tracers are naturally more highly biased. Early clustering measurements also indicated that galaxy bias cannot be linear (Gaztanaga 1992; Fry & Gaztanaga 1993). Indeed, a linear bias relation could not be preserved through the non-linear growth of structure, and analytic models (e.g. Mo & White 1996) and *N*-body simulations (e.g. Guo & Jing 2009) provide a description of this non-linearity. Biasing is also likely to be stochastic (Dekel & Lahav 1999) since it is not possible to specify the galaxy distribution without also specifying other 'hidden variables' such as luminosity, temperature, physical size, etc., which would cause some physical scatter in the relation between the galaxy and matter density fields. Additionally, stochasticity is introduced into the measurement because of the discrete samples of the density field selected, i.e. 'shot noise'. Galaxy biasing evolves with redshift (Nusser & Davis 1994; Fry 1996; Tegmark & Peebles 1998), being naturally larger at high redshift as the first galaxies to form would have done so in the densest regions. It is also scale dependent at small physical scales where the non-linear effects of galaxy formation are important, although this is weak on large scales (Mann, Peacock & Heavens 1998), being approximately scale invariant above 20–40 Mpc h^{-1} (Crocce et al. 2015). Clerkin et al. (2015) parametrized the redshift dependence of galaxy biasing. Biasing can also be expressed as a more general expansion in functions of the density field, and the related bias renormalization (McDonald & Roy 2009; Assassi et al. 2014). Galaxy bias has also been formulated in terms of the 'effective field theory of LSS' (Angulo et al. 2015).

Another popular approach, motivated by our modern understanding of galaxy formation in LCDM universes, is to parametrize the relationship between galaxies and the DM distribution assuming that all galaxies live in DM haloes or subhaloes, discussed e.g. in Tinker et al. (2010) and earlier references therein. The connection between galaxies and DM haloes can be specified by the halo occupation distribution (HOD), the probability distribution of the number of galaxies given the properties of the containing haloes, such as their masses, and given the relation between galaxy and DM spatial and velocity radial distributions. The HOD can also be studied for particular galaxy types, classified according to properties such as luminosity, stellar mass, colour and star formation rate. At low redshift this has been used with great success in SDSS, to the extent of isolating which galaxy properties are correlated with each other and with their host DM haloes, which in turn has cleanly narrowed down the wide range of suggested causes of various properties. At higher redshift, where the galaxies are less evolved and more gas rich, and where other energy inputs differ (e.g. there is more quasar activity), the picture will likely be different, and sewing it together with the low-redshift universe will likely also lead to new and interesting insight on galaxy properties and evolution. DES is ideal to pursue such studies and to push previous results based on SDSS to higher redshifts. Key constraints on the HOD of galaxies come from their clustering properties, including the angular two- and three-point cross-correlation functions, as well as from the galaxy mass correlation function and the relationship of galaxies to clusters and to underdense regions. The DES data will be powerful in constraining halo model parameters such as the occupation number and the density profile as well as determining whether the halo occupation depends on halo properties other than the halo mass.

In the context of DES, there are several approaches to quantifying biasing. These include (i) assuming an underlying model for the clustering of DM from an analytic model or simulations. The galaxy biasing can then be derived from DES clustering of galaxies (by type), e.g. from the respective two-point correlation functions: $b^2 = \xi_{\rm gg}/\xi_{\rm mm}$. See application to SV data in Crocce et al. (2016, while biasing was derived there for a magnitude-limited galaxy sample, future work will also apply it to volume-limited samples). The measurement can be generalized for halo model parameters. (ii) Using maps of DM itself. The weak lensing from DES itself can be turned into convergence (kappa) maps (Chang et al. 2015; Vikram et al. 2015), which effectively is the integral of the DM fluctuations along the line of sight (weighted by a lensing kernel). Biasing (for a magnitude-limited sample) was derived recently by Chang et al. (2016). Similarly, mass maps were derived from the fluctuations of the cosmic microwave background (CMB) by *Planck* and SPT. Cross-correlations of the DES galaxies with such mass maps can tell us the biasing (Giannantonio et al. 2016). Alternatively, it can be derived from 'counts in cells', so getting the biasing $b = \delta_{\rm g}/\delta_{\rm m}$, 'localized' over the redshift range probed by the relevant lensing kernel.

DES will also have significant power to constrain the bias and the relationship between galaxies and haloes through combinations of various observables, including galaxy–galaxy lensing, the connection between galaxies and clusters, and the connection between galaxies and underdense regions.

6.9 Galaxy intrinsic alignments

Weak gravitational lensing is a key DES cosmology probe. It uses the coherent distortion of galaxy shapes due to gravitational lensing by LSS, to measure both cosmic expansion history and the growth of structure over time. Even without this lensing effect, it is believed that intrinsic (i.e. unlensed) galaxy orientations and shapes are aligned to some extent because neighbouring galaxies form in the same large-scale gravitational potential. See Troxel & Ishak (2015), Joachimi et al. (2015), Kiessling et al. (2015) and Kirk et al. (2015) for recent reviews of the topic of galaxy alignments.

This *intrinsic alignment* (IA) of galaxies acts as a contaminant to weak lensing studies because the IA effect mimics the lensing signal, meaning that the observed cosmic shear is the sum of both contributions. Unless IAs are properly accounted for, any cosmological constraints will suffer bias, often at a very significant level. In the full DES survey, taken as a single data set, the impact of IAs is forecast to be important, contributing up to 10 per cent of total observed cosmic shear at some scales. In the type of tomographic analysis that produces useful cosmological constraints, IAs become critically important; they are forecast to contribute over 50 per cent

of the observed cosmic shear signal in some tomographic bin pairs, at some scales (Joachimi & Bridle 2010).

The IA of galaxy shapes is, however, much more than a nuisance in the pursuit of the measurement of DE. Shape, orientation or spin alignments can tell us a lot about the nature of galaxy formation and evolution, as well as shedding light on the relation between the baryonic component and its host DM haloes and helping us to understand the morphology of the cosmic web. In general, different physical alignment mechanisms are believed to be the source of IAs in red and blue galaxies, while IAs may also vary as a function of redshift, luminosity and other properties.

Most studies which set out to directly measure IAs used a sample of galaxies with spectroscopic redshifts, of which at least some subset had good shape measurements (Hirata et al. 2007; Mandelbaum et al. 2013; Singh, Mandelbaum & More 2015). A common method is to measure the two-point correlation of galaxy position with the component of galaxy ellipticity along the line of sight connecting a galaxy pair, w_{g+} (e.g. Singh et al. 2015). The relative inaccuracy of the photometric redshifts from DES make precise measurement of this statistic challenging, though Joachimi et al. (2011) demonstrated that it was possible to make measurements of large-scale IAs using data with photometric-quality redshifts. They made a positive detection of IAs in a sample of Luminous Red Galaxies (LRGs) with errors of <10 per cent using the galaxy position–ellipticity cross-correlation. DES has derived very accurate photometric redshifts for red galaxies using the redmapper (Rykoff et al. 2016) and redmagic samples, with scatter of $0.017(1+z)$ for this sample; this will enable tighter constraints. The photo-z estimates are expected to be less accurate for other galaxy samples, but even here DES offers the chance to push to redshifts deeper than the $z < 0.7$ used in this previous work. We could also employ tomographic galaxy–galaxy lensing (e.g. Blazek et al. 2012) to measure IA with the typical lensing sources.

Heymans et al. (2013) showed that a dedicated cosmic shear survey can make informative indirect measurements of IAs. Here the authors assumed a model for IAs, the non-linear alignment model of IAs (Bridle & King 2007), which has been shown to fit well at linear and quasi-linear scales. Using two-point ellipticity correlation function data from the CFHTLenS survey, Heymans et al. (2013) made a simultaneous fit to cosmological parameters and their IA model, which they parametrized by a single free amplitude parameter. Split by colour, the analysis showed that the IA of blue galaxies was consistent with zero, while IAs in red galaxies were detected at close to 2σ confidence. Both results are consistent with theoretical expectations. DES SV data are broadly comparable to CFHTLenS in terms of sky coverage and depth. The full DES 5 yr survey will increase the available area by more than a factor of 30, making it realistic to expect constraints on IA amplitude which are an order of magnitude tighter than those from CFHTLenS.

This increased constraining power will also allow more ambitious parametrizations of the IA model and the comparison of different models. Of particular interest are measurements of the IA signal as a function of luminosity, where a positive correlation has been reported, and redshift, where no evidence for evolution has been found (Singh et al. 2015). In particular, the deep redshift baseline of DES, compared to the spectroscopic data sets mostly used in the past, is likely to improve knowledge of IA evolution; this is of importance in understanding the mechanisms which source galaxy shape alignments.

The DES data set will be extremely useful for joint studies of IAs in combination with data from other surveys. Overlapping spectroscopic surveys (see Fig. 1) combined with high-quality shape measurements from DES will allow for high-precision IA measurements. In the future, the Sqaure Kilometere Array (SKA) large volume radio survey offers potentially novel synergies, including the comparison of shape measurements made in the optical and radio wavelengths (Brown et al. 2014), large numbers of spectroscopic-quality redshifts from the H I survey (Abdalla et al. 2015), and potentially the use of radio polarization or radial velocity measurements to directly access information about the intrinsic galaxy ellipticity, allowing for the calibration of IAs in optical surveys such as DES (Whittaker, Brown & Battye 2015). Cross-correlating lensing maps derived from the CMB (which are not affected by IA) with those from galaxy shapes measured in DES will allow a novel measurement of IAs (e.g. Kirk et al. 2016).

7 CLUSTER PROPERTIES

In addition to their roles as cosmological probes, clusters of galaxies offer important insights into a slew of astrophysical processes including the formation and evolution of galaxies, the effects of AGN feedback, tests of the nature of DM, the acceleration of relativistic particles and the amplification of magnetic fields (among other astrophysical plasma processes). Their deep DM potential wells retain baryons, allowing multiple cold and hot phase baryonic components to be observed. They are also powerful gravitational lenses offering probes of the mass and structure of the clusters themselves as well as the magnification of very high redshift galaxies and quasars, allowing study of these very distant objects. DES will detect of the order of 100 000 clusters out to $z \sim 1$, comparable to the number of haloes with masses above 10^{14} $M_{\odot}$ expected in an LCDM universe over this sky area (Allen, Evrard & Mantz 2011).

Overlap with the SPT provides around 1000 clusters detected via the Sunyaev–Zel'dovich (SZ) effect between the existing 2500 sq deg survey and a nearly complete SPTpol survey; thousands more are expected from the upcoming SPT-3G survey. Existing *XMM–Newton* and *Chandra* data likewise give X-ray coverage of approximately 1000 clusters. For these samples, DES provides both photometric redshifts and cluster confirmation through the existence of galaxy overdensities, and this overlap enables multiwavelength probes of cluster and cluster galaxy evolution.

Clusters also act as signposts of the cosmic web, and both the large-scale galaxy distribution and weak lensing shear signal from DES data will allow the identification of supercluster and void regions and filaments joining clusters (Vikram et al. 2015). This in turn will allow tests of structure formation and galaxy evolution models as well as potentially identifying sightlines for searches for absorption due to the warm–hot intergalactic medium (e.g. Tejos et al. 2016).

The effects of environment on galaxy evolution, the properties of galaxies in clusters and the formation of massive cluster central galaxies have already been discussed in Section 5. Here we focus on additional science with DES clusters and existing auxiliary data.

7.1 Cluster evolution

DES data (optical richness + ICL and lensing masses) coupled with X-ray and/or SZ samples of the hot gas phase will enable the study of the full baryonic content of massive haloes. The combined data will enable the study of the joint scalings of stellar mass, gas mass, gas temperature, X-ray luminosity, etc. with halo mass and redshift. In particular, the data should allow the covariance of these properties at fixed halo mass to be determined with significantly higher precision (Evrard et al. 2014). In cosmological hydrodynamic simulations, the statistical relationships among stellar and hot phase

properties are sensitive to the details of the 'subgrid' astrophysical models employed for star and supermassive black hole formation and their attendant feedback channels. Empirical constraints from DES studies will thereby lead to improved subgrid prescriptions in simulations.

DES will also enable the study of cluster properties as a function of formation epoch and dynamical state, and will identify potentially early forming systems such as fossil groups (e.g. Jones et al. 2003). Cluster formation epoch is thought to be an important additional parameter affecting the observed properties of clusters, such as richness, and contributing to the scatter in cluster scaling relations (Mao, Williamson & Wechsler 2015). Indicators for cluster formation epoch that can be probed by DES include the magnitude gap between the brightest and next brightest cluster galaxies, the luminosity of the brightest galaxy, and the offset between the brightest galaxy and the light-weighted mean galaxy position (Raouf et al. 2014). These measures can be used to correlate cluster richness and multiwavelength properties to cluster formation time.

In addition, DES will allow studies of the stellar mass fraction in clusters. This has already been done with early DES data in Palmese et al. (2016), where they derived the stellar mass profile for the cluster RXC J2248.7−4431, and compared it with the total mass derived from DES weak lensing analysis, resulting in a stellar mass fraction of ∼0.7 per cent within $r_{200c} \approx 3$ Mpc. This and similar techniques will be applied to $\sim 10^5$ DES clusters to provide important information about galaxy evolution.

7.2 AGN evolution and feedback

In addition to the evolution of galaxies and their SFHs as a function of environment, DES will also enable studies of AGN activity and studies of correlations between AGN activity and environment, galaxy and host cluster properties. Many observational lines of evidence point to a strong connection between supermassive black hole growth, star formation and galaxy growth, including a similar evolution in AGN activity and star formation out to $z \sim 2$ (e.g. Boyle & Terlevich 1998; Franceschini et al. 1999; Merloni, Rudnick & Di Matteo 2004; Silverman et al. 2008) and the correlation between black hole mass and the velocity dispersion of the host galaxy's central bulge (e.g. Ferrarese & Merritt 2000; Gebhardt et al. 2000; Tremaine et al. 2002). AGN feedback is critical in balancing cooling and regulating star formation in both cluster cores and in galaxies; it is also clear that some form of non-gravitational heating is necessary out to large radii in clusters to explain the observed deviation of cluster scaling relations (such as the relation between the X-ray luminosity and the temperature of the intracluster medium) from the expected self-similar form (e.g. Markevitch 1998; Arnaud & Evrard 1999).

DES will enable studies of the connection of AGN activity to cluster and galaxy evolution with a large sample over a large redshift baseline, particularly in conjunction with existing X-ray and radio data. Importantly, DES provides the ability to connect AGN activity to both galaxy environment and star formation.

The population of AGN in clusters (both in central and satellite galaxies) compared to the field offers valuable information on AGN fuelling and the connection of AGN to galaxy evolution. Previous studies indicate a very strong evolution in the fraction of cluster galaxies hosting X-ray detected AGN as a function of redshift with the cluster AGN fraction increasing by a factor of 30 between $z \sim 0.2$ and $z > 1$ (e.g. Martini, Sivakoff & Mulchaey 2009; Martini et al. 2013). This evolution is stronger than the evolution in the field AGN fraction so that at high redshift the cluster and field AGN fractions become comparable whereas at low redshift AGN are more common in field galaxies (Martini et al. 2013). This rapid evolution in cluster AGN activity parallels a similar evolution in the fraction of star-forming galaxies in clusters over the same epoch (e.g. Haines et al. 2009). In addition, there are some indications that groups and smaller mass clusters at low redshifts host a higher AGN fraction than massive clusters (Arnold et al. 2009). These previous studies are based on relatively small cluster and AGN samples. Larger samples of cluster AGN are already available in the relatively small area of DES SV with overlapping *Chandra* archival data, and preliminary results indicate a similar strong redshift evolution in the cluster AGN fraction (Bufanda et al., in preparation). The DES cluster sample will also provide a much larger cluster mass range over which to study the correlation of AGN activity to host halo mass.

7.3 Cluster sub-populations

DES will discover new clusters suitable for many diverse science programmes and will have the statistics to identify samples of relatively rare sources. DES will, therefore, provide follow-up targets for a wide variety of programmes including the following.

Merging clusters. DES cluster samples combined with DES weak lensing and/or existing X-ray and SZ data will allow the identification of new bullet cluster-like systems suitable for tests of DM self-interaction (e.g. Markevitch et al. 2004; Harvey et al. 2015). The strong correlation of diffuse synchrotron radio emission with cluster merging activity (e.g. Cassano et al. 2013; Cuciti et al. 2015) also shows that energetic cluster mergers are effective particle accelerators; however, the mechanisms responsible, whether shock acceleration, turbulent re-acceleration or secondary hadronic production, are still poorly understood. Ongoing and upcoming surveys with the Low Frequency Array (van Haarlem et al. 2013) and Australian Square Kilometre Array Pathfinder (Norris et al. 2011) are expected to allow the first large population studies of diffuse cluster radio sources; the properties, particularly in terms of dynamical state, that are correlated with whether DES clusters host large-scale radio emission or not will help illuminate the mechanisms responsible for particle acceleration in clusters and the lifetime of diffuse radio emission.

Relaxed clusters. The identification of the most relaxed clusters, particularly at high redshifts, is important both for cosmological studies and for understanding the balance of heating and cooling in the intracluster medium (ICM). The fraction of cluster mass in baryons gives a standard ruler by which the DE density and other cosmological parameters can be constrained; this method requires identifying relaxed clusters (which are relatively free of biases due to asymmetry and lack of hydrostatic equilibrium) over a large redshift baseline for deep X-ray follow-up (e.g. Allen et al. 2008). As highlighted above, the history of cooling and AGN feedback in cluster cores shape the evolution of the ICM. Current evidence points to a lack of strong cool cores at higher redshifts (e.g. McDonald et al. 2013, 2014), but larger samples and further study are needed to confirm this trend. Strong cool-core clusters such as the Phoenix cluster (SPT-CL J2344−4243; McDonald et al. 2012) stand out in the DES data as rich clusters with blue, star-forming central galaxies. The DES data will also allow studies of the central galaxy properties of cool-core clusters identified in X-ray or SZ.

High-redshift clusters. In combination with existing infrared surveys such as *Spitzer* Infrared Array Camera and *WISE* within the DES survey area, we will also be able to detect very high redshift clusters in the range $z = 1.0$–1.5 and possibly beyond. The very

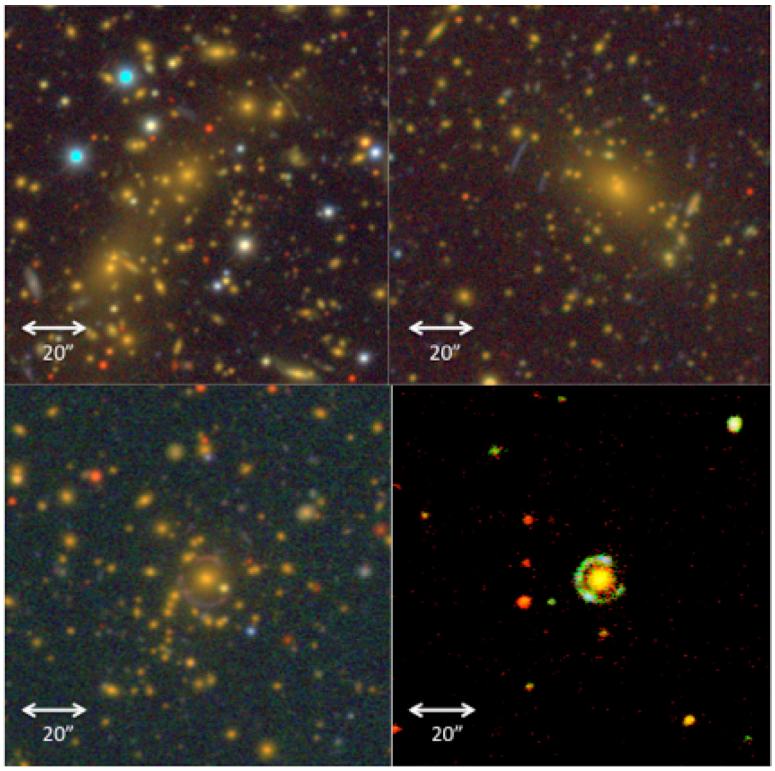

Figure 12. Four examples of known strong lensing systems from DES SV and Y1 data.

deep data which DES is acquiring in the SN fields will also provide additional leverage for high-redshift cluster science. This sample will allow the study of clusters near the epoch of their formation. Little is known about clusters at redshifts much higher than $z \sim 1$ as only small samples of very high redshift clusters have been identified thus far, and the discovery of new high-redshift clusters by DES will have significant impact. These clusters will allow us to extend many of the above-mentioned studies to higher redshifts. For example, while we observe significant evolution in the properties of cluster galaxies and the ICM from the present epoch out to $z \sim 1$, many of the bulk cluster properties are already in place. To understand questions of ICM heating, the establishment of the red sequence and BCG formation, it is advantageous to push our observations closer to cluster formation.

8 STRONG GRAVITATIONAL LENSING

DES expects to discover many new strongly lensed galaxies and quasars. A simple extrapolation from the CFHTLS-Strong Lensing Legacy Survey [using the 54 systems with rank 3 and above from More et al. (2012) and adjusting for the different survey depths] predicts that the wide survey will contain of the order of 1000 lenses with 18 arcsec $> \theta_{\rm E} >$ 2 arcsec (where $\theta_{\rm E}$ is the Einstein radius) of which about 200 would contain giant arcs (with arc length-to-width ratio >8). A more rigorous prediction for galaxy-scale lenses (Collett 2015) suggests that we might discover of the order of 800 lenses with $\theta_{\rm E}$ centred at about 1.5 arcsec using difference imaging between the *g* band and the appropriately scaled *i* band, as described in Gavazzi et al. (2014). In addition, we also expect to find a sample of ∼120 lensed quasars brighter than $i = 21$ (Oguri & Marshall 2010), including 20 quadruples with high information content (we note that by "brighter than $i = 21$" they define their limit in terms of the fainter component of pairs and third brightest components for quads).

We are adopting a multipronged approach to identifying strong lenses in DES. To select lensed galaxies, we will use a combination of automated arc-finders (e.g. More et al. 2012; Gavazzi et al. 2014), catalogue searches (e.g. Kubik 2007; Belokurov et al. 2009; Kubo et al. 2010) and crowd-sourced citizen-science efforts (Marshall et al. 2016). All of these have in common at least some amount of visual scanning as the final step in the search process. Examples of some known strong lenses in the DES footprint are shown in Fig. 12. The lensed quasar search will use colour and morphology information at the catalogue level as well as the variable nature of quasars. We have no *u*-band observations in DES, so to compensate we will need to use infrared bands, e.g. *WISE*. We have already carried out spectroscopic follow-up of some lens candidates from the DES SV data and have confirmed a number of systems (Nord et al. 2015). In addition, we have confirmed the first lensed quasars in DES, identified using the colour and morphology information (Agnello et al. 2015).

We will be able to use the sample of strongly lensed systems to study DM mass profiles at scales from individual galaxies all the way to massive clusters. Cluster-scale lenses are particularly useful because they allow us to study the effects of strong lensing in the core of the cluster and weak lensing in the outer regions. Strong lensing provides constraints on the mass contained within the Einstein radius of the arcs whereas weak lensing provides information on the mass profiles in the outer reaches of the cluster. Combining the two measurements allows us to make tighter constraints on the mass and the concentration of an Navarro–Frenk–White (Navarro, Frenk & White 1997) model of the cluster mass density profile over a wider range of radii than would be possible with either method alone (Natarajan et al. 1998, 2002; Bradač et al. 2006, 2008a,b; Diego et al. 2007; Hicks et al. 2007; Limousin et al. 2007; Deb,

Goldberg & Ramdass 2008; Merten et al. 2009; Oguri et al. 2009). In addition, if one has spectroscopic redshifts for the member galaxies, one can determine the cluster velocity dispersion, assuming that the cluster is virialized, and hence obtain an independent estimate for the cluster mass (Becker et al. 2007). These different methods, strong plus weak lensing and cluster velocity dispersion, provide independent estimates of the cluster mass and can then be combined to obtain improved constraints on the mass and concentration (e.g. Buckley-Geer et al. 2011). Galaxy-scale lenses with multiple source planes (Gavazzi et al. 2008) also provide excellent constraints on the DM distribution in galaxies (Sonnenfeld et al. 2012), which is a sensitive test of galaxy formation models and baryonic feedback processes (Johansson, Naab & Ostriker 2012).

We will have a large sample of sources at varying redshifts which will be very valuable for studies of galaxy evolution (e.g. Saintonge et al. 2013; Bayliss et al. 2014; Genzel et al. 2014; Rhoads et al. 2014). For example, Collett (2015) predicts that the source redshift distribution for galaxy-scale lenses peaks at about $z_s = 2.0$. Strongly lensed galaxies are particularly useful for the study of high-redshift galaxies due to the magnification of the galaxy flux. Therefore, lensed galaxies are prime candidates for detailed studies, since they can be investigated using only a fraction of the telescope time that would be needed to study comparably distant but unmagnified galaxies. Moreover, since lensing increases the apparent angular size of the source, it enables the study of source galaxy substructure with greater effective spatial resolution than for an unlensed source of the same physical size at comparable distance. The excellent red sensitivity of the DECam CCDs, along with the *grizY* filter set, provides sensitivity to high-redshift LBGs (e.g. *g*-band dropouts at $z \sim 4$ or *r*-band dropouts at $z \sim 5$).

One of the primary motivations for the lensed quasar search is cosmology (e.g. Suyu et al. 2013). However, considerable additional science can be carried out using these systems. For example, stars in the lens cause microlensing effects on the multiple quasar images, which can be used to examine the stellar contents of the lens galaxy (e.g. Oguri, Rusu & Falco 2014; Schechter et al. 2014; Jiménez-Vicente et al. 2015). The same microlensing can also provide constraints on the inner structure of the lensed quasar, such as the size of the accretion disc and the thermal profile (e.g. Poindexter, Morgan & Kochanek 2008) as well as the geometry of the broad-line region (e.g. Sluse et al. 2011). In addition, milli-lensing caused by flux ratio anomalies probes the presence of substructure in the lens (e.g. Nierenberg et al. 2014). Finally, using high-resolution imaging of the lens allows the reconstruction of the source and can provide a direct view of quasar host coevolution up to $z \sim 2$ (e.g. Peng et al. 2006; Rusu et al. 2016).

9 QUASARS

The DES photometric data will contain millions of new quasars (QSOs), and in particular new samples at $z > 6$ and $z > 7$ that can be used to study the reionization history of the Universe through measurements of the transparency of the intergalactic medium (IGM), the evolution of supermassive black hole masses, the chemical evolution of the IGM from the statistics of metal-line absorption systems, their space density evolution and many other topics. In addition, the regular monitoring cadence employed for the SN survey will include variability data that can be used to estimate supermassive black hole masses via the reverberation mapping technique, as well as to select quasar candidates. Fig. 13 shows a DES colour–colour diagram, as well as known quasars overlapping the DES SV observations.

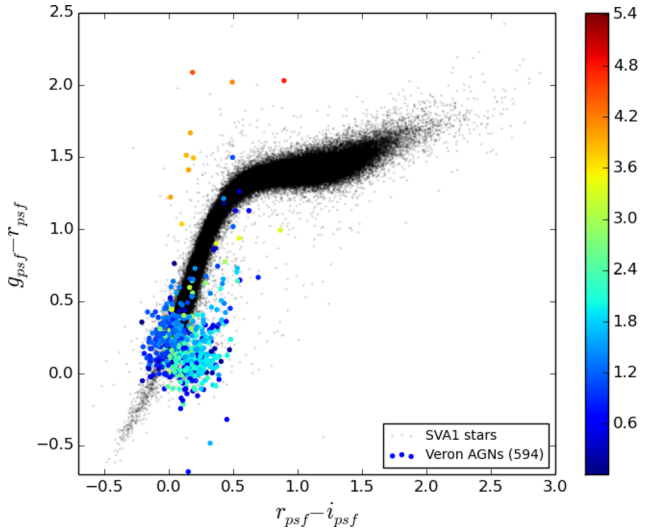

Figure 13. DES *gri* colour–colour diagram showing the stellar locus as well as known quasars overlapping the DES SV observations. The quasars have been colour-coded according to redshift. While the low-redshift quasars overlap the stellar locus, the $z > 4$ quasars clearly appear as very red ($g - r$) sources.

9.1 Expected numbers of quasars

We have constructed mock quasar catalogues for DES using the quasar SED models of Maddox et al. (2008, 2012) and the quasar luminosity functions from Ahn et al. (2012) at $z < 5$, McGreer et al. (2013) at $5 < z < 6$ and Willott et al. (2010) at $z > 6$. Based on these luminosity functions (or extrapolations at high redshifts assuming pure density evolution), we can calculate the total number of quasars over various redshift ranges that can be expected in the DES volume. Illustrative sample sizes of photometrically selected quasars over the DES wide-survey area of 5000 sq deg and down to the typical 10σ point source depths include 670 000 with $i_{AB} < 24.0$ at $2 < z < 4$, 33 000 with $z_{AB} < 23.4$ at $4 < z < 5$, 370 with $z_{AB} < 23.4$ at $6 < z < 7$ and 5 with $Y_{AB} < 21.7$ at $z > 7$.

In addition, the DES-SN fields covering ∼27 sq deg are imaged to much fainter magnitude limits. Although DES lacks *u*-band coverage, the *grizY* filters can effectively be used for the selection of faint $z > 4$ quasars (which appear as *g*-band dropouts) and $z > 5$ quasars (which appear as *r*-band dropouts). Down to a 5σ depth of $z < 26.5$, we expect ∼840 quasars at $4 < z < 5$ and ∼390 quasars at $5 < z < 6$ in the DES-SN fields. At these magnitude limits, the faint quasar population begins to overlap the bright end of the LBG population, thus potentially enabling constraints on the relative space densities of the brightest star-forming galaxies and the faintest AGNs observable at high redshifts.

9.2 Quasars at the epoch of reionization

The very deep *z*-band data obtained as part of DES, combined with *Y*-band observations, make the DES data particularly well suited for the discovery of new quasars at redshifts of six and above. At these redshifts, quasars may be selected as *i*-band dropouts, or even *z*-band dropouts. The source of confusion for these dropout samples is very red Galactic stars and substellar objects, namely L and T dwarfs (Fan et al. 2001, 2006), which have substantially higher surface densities at these magnitude limits. Quasars may be separated from stellar objects in colour space with the addition of a redder filter, as the intrinsic SED of quasars is generally much bluer

than these Galactic objects. For $z \sim 6$ quasars, $z - Y$ colours are an effective discriminant, while for the $z \sim 7$ quasars that will be z-band dropouts (Mortlock et al. 2011), J-band observations from VHS and VIKING will be used.

Reed et al. (2015) illustrated the promise of quasar discovery with DES with the discovery of a quasar at $z > 6$. The quasar was the brightest of 43 candidates and was identified for follow-up work solely on the DES $i - z$ and $z - Y$ colours. Spectroscopy of the quasar, DES J0454−4448, showed that it has an emission redshift of $z = 6.10 \pm 0.03$ and an H I near zone size of 4.6 ± 1.7 Mpc. The presence of one $z > 6$ quasar in the relatively small area probed by the DES SV data is consistent with the luminosity function expected at $z \sim 6$.

Quasars at redshifts below six show a substantial amount of Lyman α absorption due to intervening neutral hydrogen gas at lower redshift, yet the transmission of some quasar continuum below the break indicates that the IGM is mostly ionized. In contrast, quasars at redshift six and above exhibit complete Gunn–Peterson absorption troughs (Gunn & Peterson 1965) that indicate that the optical depth is much greater than one and imply a significant change in the neutral fraction (Fan et al. 2002, 2006; Meiksin 2009). However, the present data are unable to differentiate between a neutral fraction of 1 and 100 per cent, or whether there are comparable volume fractions at these two extremes. In addition to the evidence for a global increase in the neutral fraction, some sightlines show regions with substantial transmitted flux above redshift six (White et al. 2003). This variable optical depth is expected from models of reionization, which predict substantial variations in the neutral fraction when the Strömgren spheres are growing, but do not yet overlap (e.g. Furlanetto, Zaldarriaga & Hernquist 2004; Furlanetto 2009). The new, bright quasars discovered with DES will be valuable for improved determinations of the patchiness of the ionization fraction above redshift six, the space density of the sources that produce reionization, whether reionization begins in overdense or underdense regions, and the physical state of the IGM.

9.3 Space density evolution

Another interesting result to arise from the study of quasars at $z > 2.9$ is that their correlation lengths are as large as those for massive clusters of galaxies in the local universe, and well above those measured for local quasars (Shen et al. 2007). As the quasar space density also declines dramatically at $z > 2.9$ (Warren, Hewett & Osmer 1994; Schmidt, Schneider & Gunn 1995; Richards et al. 2006), the combination of very low space density and very large correlation length provides very strong constraints on the fraction of the time galaxies appear as quasars (the duty cycle) and the mass accretion history of their supermassive black holes (Cole & Kaiser 1989; Haiman & Hui 2001; Martini & Weinberg 2001). These measurements also place a strong constraint on the maximum amount of scatter between quasar luminosity and halo mass (White, Martini & Cohn 2008). Shankar et al. (2010) found that a model with the duty cycle equal to 0.2, 0.5 and 0.9 at redshift 3.1, 4.5 and 6.0 respectively provides the best match to the clustering and space density data. In the context of their model, part of the reason that the quasar space density drops precipitously between redshift three and six is because sufficiently massive haloes are progressively more rare, yet the rate of this decline is partially compensated by the increase in the duty cycle. As the duty cycle cannot exceed unity, the decline in the quasar space density above redshift six is predicted to be yet more precipitous because it will be forced to track more exactly the evolution of the most massive haloes. This space density decline above redshift six is approximately a factor of 3 faster than a simple extrapolation of the space density evolution from three to six. The discovery of a substantial number of quasars at redshift seven, and the first measurement of the quasar space density at this redshift, will provide a powerful test of this model prediction and thereby shed light on the relationship between massive haloes and quasars at the highest redshifts.

9.4 Black hole mass calibration via reverberation mapping

A fundamental challenge for studies of the evolution of supermassive black holes is accurate estimates of their masses. Dynamical measurements of supermassive black hole masses are possible for quiescent galaxies at distances up to about 100 Mpc for the largest telescopes working near the diffraction limit (McConnell et al. 2012). However, similar measurements are not feasible for objects at larger distances, and especially not cosmological distances ($z > 0.1$), and there are thus no direct, dynamical measurements of how supermassive black holes grow over cosmic time. The best objects to use in the study of the evolution of supermassive black hole mass are broad-line AGN, which can be observed to the highest redshifts. Reverberation mapping (Blandford & McKee 1982; Peterson 1993) provides the most direct measurement of black hole mass for AGN. This technique employs measurements of the velocity width of a broad emission line and the time lag between continuum and line luminosity variations. The time lag provides the size scale of the broad-line region, and combined with the velocity width of the broad line provides a measurement of the enclosed (black hole) mass. While there are inherent uncertainties due to the geometry and dynamics of the broad-line region (Horne et al. 2004; Collin et al. 2006; Pancoast, Brewer & Treu 2014), these measurements agree well with mass estimates based on stellar kinematics (Ferrarese et al. 2001; Onken et al. 2014) and have been used to develop empirical relationships between continuum luminosity (which is used as a proxy for broad-line region size) and line width that have been employed to estimate the evolution of supermassive black holes over cosmic time (Kaspi et al. 2002; McLure & Dunlop 2004; Kollmeier et al. 2006; Vestergaard & Peterson 2006; Vestergaard & Osmer 2009). The key uncertainty in this extrapolation to high redshifts is that the local AGN studied via reverberation mapping have almost exclusively been low-luminosity objects (Dasyra et al. 2007; Del Moro et al. 2008; Bentz et al. 2013; Bentz & Katz 2015), while studies of black hole evolution employ quasars that are an order of magnitude more luminous. This is both because of the scarcity of truly luminous AGN in the local universe and because the variable time-scales for such AGN are substantially longer and consequently present a greater practical challenge. The 27 sq deg DES-SN survey is well suited to measure black hole masses for higher luminosity and higher redshifts due to the regular cadence of photometric observations for 5 years, combined with approximately monthly spectroscopic follow-up observations as part of the OzDES survey (Yuan et al. 2015) on the Anglo-Australian Telescope. There are several thousand quasars in this area with $0.1 < z < 4$ and $i < 21$ mag, and the DES observations of the SN fields provide regular monitoring of them for the substantial continuum variations that provide a strong reverberation signal. At the same time, regular spectroscopic follow-up observations of ∼800 of these quasars obtained as part of the OzDES survey will be used to measure the corresponding emission-line flux variation and thus the size of the broad-line region. Based on detailed simulations of this survey by King et al. (2015), we expect to recover lags for 35–45 per cent of these quasars. Reverberation-based black hole masses for even

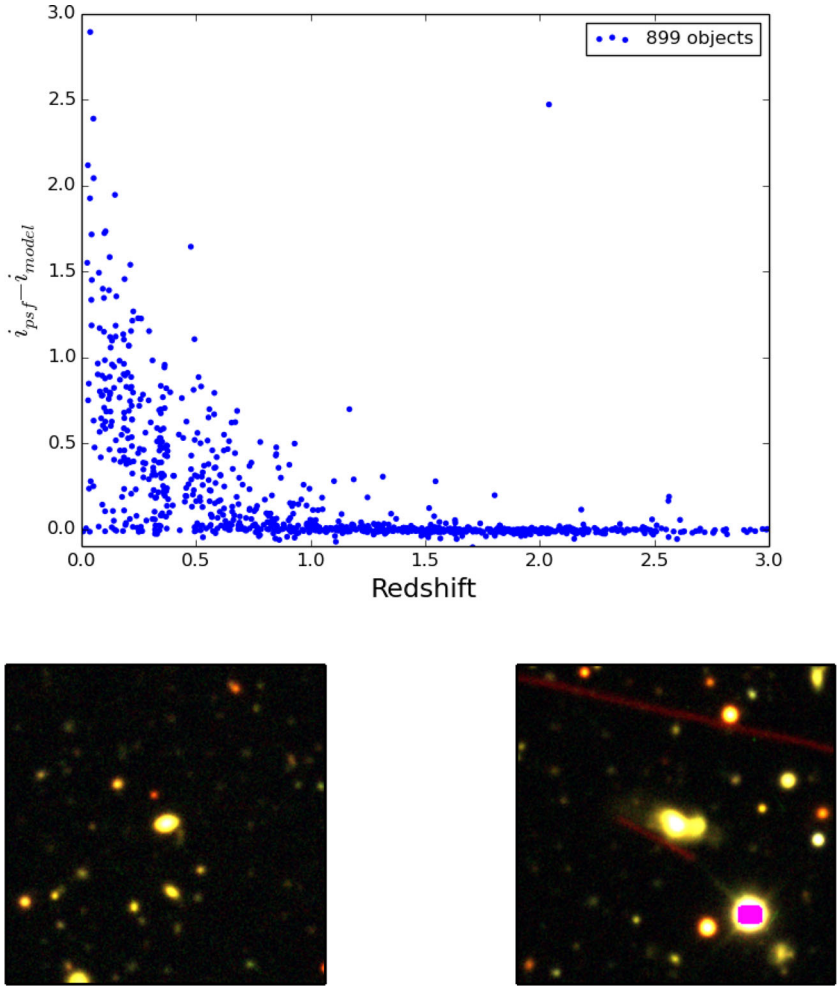

Figure 14. Extended objects can be identified by comparing the PSF magnitude to the model magnitude. Top: the figure shows that many quasars in our sample are resolved (appear to be extended objects) even out to $z \sim 1.0$. Bottom: DES *gri* colour-composite images of two known quasars at $z = 0.85$ (left) and $z = 1.17$ (right). Both quasars have extended morphologies in the DES data demonstrating that low surface brightness host galaxy features are clearly visible for quasars out to $z \sim 1$.

a small fraction of these quasars would substantially increase the present sample of approximately ∼70 AGN with such data (Bentz et al. 2010; Grier et al. 2012; Barth et al. 2015; Bentz & Katz 2015), as well as populate the largely unconstrained parameter space at high luminosities.

9.5 Quasar host galaxies

One of the main questions in AGN research concerns how supermassive black holes are fuelled. For luminous quasars, the necessary fuel supply is substantial (a few $M_\odot$ yr^{-1}) and estimates of the typical quasar lifetime suggest that this accretion rate is maintained for $\sim 10^{7-8}$ yr (Martini 2004). Gas-rich galaxy mergers appear to be the most viable fuelling mechanism (e.g. Di Matteo, Springel & Hernquist 2005; Hopkins et al. 2008) in galaxy formation models. However, observational evidence for quasars being hosted in merging galaxies has proved elusive, particularly at high redshifts. This is largely because the bright quasar emission makes it challenging to classify the host galaxy morphology in all cases, as well as because of the absence of a comparison sample to quantify the incidence of mergers. Data from DES can help to address both of these issues. DES data will allow us to resolve low surface brightness features far from the quasar nuclear flux. A census of merging systems in non-quasar hosts over the same redshift range can also be extracted from the DES data and used as a control sample. This control sample is important to quantify the fraction of all mergers that are detectable at the larger radii probed by quasar hosts. Fig. 14 shows the difference between the point spread function (PSF) and model magnitude in the *i* band for a sample of known luminous quasars overlapping DES SV data from Veron-Cetty & Veron (1993). As the PSF magnitude only encompasses flux in the central nuclear region whereas the model magnitude is a better measure of the total flux, unresolved point sources will have a small difference between their PSF and model magnitudes whereas extended sources will have a much larger difference. The top panel of Fig. 14 shows that at high redshifts, luminous quasars are unresolved in DES data as expected. However, extended morphologies are seen for a significant number of quasar host galaxies out to $z \sim 1$. Two example DES images for $z \sim 1$ quasars are also shown in Fig. 14 and demonstrate that DES will be uniquely sensitive to quasar host galaxies at these redshifts.

Host galaxy studies will be even more viable in dust-reddened quasars (e.g. Banerji et al. 2012, 2013) where there is significant extinction towards the quasar line of sight. As these dusty quasars are thought to correspond to a phase of transition between starburst

galaxies and UV-luminous quasars, a large fraction of them are expected to be hosted in merging systems. At low redshifts, there is evidence that dust-reddened quasars do indeed reside in mergers (Urrutia, Lacy & Becker 2008) and DES will enable an extension of these studies to much higher redshifts.

10 SNE AND TRANSIENTS

The DES Supernova (DES-SN) programme was designed to discover and photometrically follow thousands of SNe Ia for cosmology (Bernstein et al. 2012). The DES-SN programme surveys 27 sq deg over 10 DECam fields (two 'deep,' eight 'shallow') chosen to overlap with well-observed fields: the ELAIS-S, XMM-LSS, CDF-S and 'Stripe-82' with the latter three also corresponding to PS1 Medium-Deep Fields. The survey has already discovered >1000 SN Ia candidates, with hundreds of host galaxy redshifts obtained via the OzDES project (see Yuan et al. 2015) and nearly 100 SNe spectroscopically classified using other 4–10 m class telescopes.

While running the SN survey, DES will naturally discover thousands of other astrophysical transients. The largest fraction should be core-collapse SNe. However, the survey will also discover many 'exotic' transients (those not falling into the normal SN classes of II, Ia, Ib or Ic). In particular, DES-SN has already discovered several superluminous SNe (SLSNe; Papadopoulos et al. 2015; Smith et al. 2016) and one tidal disruption event (TDE; Foley et al. 2015). Here we briefly outline the potential science that can be achieved with these discoveries.

As of Y3, we are now making public instantaneously all our bright ($r < 20$) transients at https://portal.nersc.gov/des-sn/ so that they can be followed up by other groups.

10.1 Core-collapse SNe

Core-collapse SNe, those SNe with massive-star progenitors that undergo a core collapse, represent roughly 75 per cent of all stellar explosions in a given volume (Li et al. 2011). However, core-collapse SNe tend to be fainter than SNe Ia, and thus only represent about 20 per cent of all discovered SNe in a magnitude-limited survey (Li et al. 2011). None the less, DES-SN should discover about 500 core-collapse SNe.

There are currently several open questions about core-collapse SNe, ranging from their precise progenitors – especially for different classes (e.g. Smartt 2009), how they explode (see Janka et al. 2007, for a review) and their connection to gamma-ray bursts (GRBs; e.g. Woosley & Bloom 2006). Furthermore, core-collapse SNe can be used to track the star formation rate history of the Universe and possibly for constraining cosmological parameters (e.g. Nugent et al. 2006).

DES-SN has already spectroscopically classified many 'typical' core-collapse SNe. DES-SN should be able to detect most core-collapse SNe out to $z \approx 0.2$. With the full photometric sample, we plan to address the above topics.

10.2 Superluminous SNe

So far DES has published results for two SLSNe. There are others confirmed spectroscopically (e.g. DES15E2mif; Pan et al. 2015) and many more candidates.

The first spectroscopically confirmed SLSNe discovered by DES (DES13S2cmm) is presented in detail in Papadopoulos et al. (2015). The event was discovered early in the first year of DES operations. Spectroscopy with the ESO Very Large Telescope showed that DES13S2cmm was spectroscopically similar to SLSN-I [meaning it lacks hydrogen; see Gal-Yam (2012) for details of SLSN classification] at $z = 0.663 \pm 0.001$ (with the redshift from host galaxy emission lines). At this redshift, the SN had a peak U-band rest-frame absolute magnitude, $M_{U,\mathrm{peak}} = -21.05^{+0.10}_{-0.09}$ mag, consistent with other SLSNe.

Like some other SLSNe (e.g. Neill et al. 2011; Lunnan et al. 2014), DES13S2cmm is located in a faint, low-metallicity (sub-solar), low-stellar-mass host galaxy with $\log(M/\mathrm{M}_{\odot}) = 9.3 \pm 0.3$ (see Lunnan et al. 2015). The bolometric light curve of DES13S2cmm is consistent with being powered by the spin-down of a magnetar, see Kasen & Bildsten (2010) and Woosley (2010), a model which can fit the basic observables of several SLSNe-I (e.g. Nicholl et al. 2014).

The second published DES SLSN is DES14X3taz (Smith et al. 2016) which is also hydrogen poor (SLSN-I) at a redshift of $z = 0.608$. The light curve of DES14X3taz is double-peaked, with the first peak being relatively blue, lasting 15 rest-frame days, with a peak luminosity of 30 per cent of the main second peak which resembles other SLSN-I in DES (Papadopoulos et al. 2015) and the literature. The discovery of double-peaked SLSN light curves provides an important insight into their possible progenitors, suggesting an initial very hot event (first peak) that cools rapidly followed by the re-heating of the very extended stellar envelope (hundreds of solar radii) by a central engine such as a magnetar. Such double-peaked SLSNe could be common as recently suggested by Smith et al. (2016) and Nicholl et al. (2015). Based on current rate estimates (Quimby et al. 2013), DES should detect between 15 and 20 SLSNe over 5 years (see Scovacricchi et al. 2016).

In Y1, we started a programme for selecting SLSN candidates from the pool of all DES-SN detected transients using the following criteria: (i) at least one month of multicolour data (typically five to six detections with S/N > 3.5 in each of *griz*); (ii) a low probability of fit to any standard type Ia, II or IIb/c light curve (Sako et al. 2014); (iii) SN located at least one DECam pixel from the centre of its host galaxy (if a host was detected); and (iv) a peak observed magnitude no fainter than 1 mag below its host galaxy (if detected). This resulted in up to 50 possible candidates which were then inspected visually to determine if their multicolour light curves were consistent with other observed SLSNe, i.e. if the rise time of the light curve was greater than 25 observer-frame days and, provided a host photometric or spectroscopic redshift was available, if the peak absolute magnitude was less than −20.5 mag. See Fig. 15 for examples of five hostless SLSN candidates from Y1.

The search for SLSN candidates continued into Y2 of the DES-SN programme and, due to increased spectroscopic follow-up time, we have spectroscopically confirmed many more SLSN candidates. New surveys such as 'Search Using DECam for Superluminous Supernovae' (SUDSS), which supplement the DES-SN data, should increase the yield of SLSNe to nearly a hundred such events out to $z \approx 2$ (Scovacricchi et al. 2016). The size and quality of such a sample should greatly improve our astrophysical knowledge of these luminous explosions.

10.3 Exotic thermonuclear transients

SNe Ia are thermonuclear explosions of C/O WDs. There are several other classes of explosions with similar origins. Of the classes which have been observed, there are the low-energy, low-luminosity SNe Iax (Foley et al. 2013), the Ca-rich SNe (Perets et al. 2010) which may come from stars ejected from their galaxies (Foley 2015), the low-velocity, low-temperature SN 2002es-like

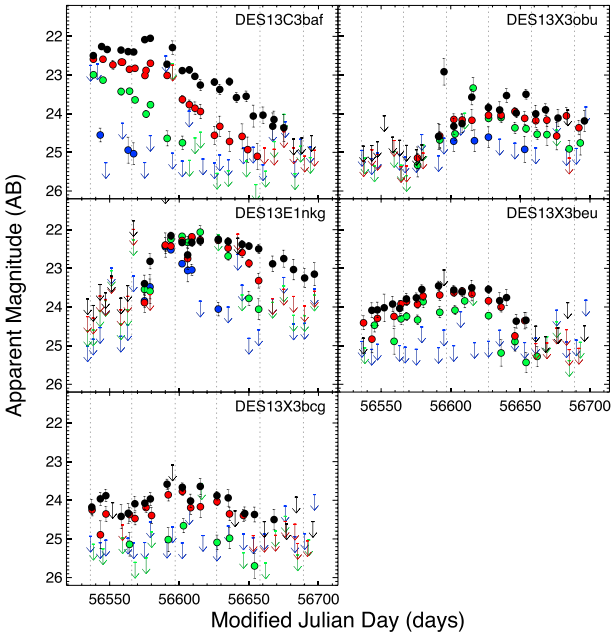

Figure 15. Examples of five hostless SLSN candidates selected from Y1 of DES. These are in addition to DES13S2cmm (Papadopoulos et al. 2015) which was spectroscopically confirmed. The long multicolour light curves of these candidates are consistent with other SLSNe and are not AGNs due to the lack of a visible host galaxy. The colours are blue (g-band), green (r-band), red (i-band) and black (z-band). Upper limits are shown as arrows.

SNe (Ganeshalingam et al. 2012), the troublesome SN 2006bt-like SNe (Foley et al. 2010) and kilonovae (which are thought to have neutron star progenitors; Berger, Fong & Chornock 2013; Tanvir et al. 2013). There are also several proposed classes such as Ia SNe (Bildsten et al. 2007).

Exotic transients are not just an idle curiosity; they are the result of the most extreme physical conditions imaginable. For instance, the above classes are the result of truly unexplored phenomena and represent new endpoints of stellar evolution and the boundaries of possible physical conditions of stellar systems. Meanwhile, the explosions probe interesting corners of physics such as r-process element creation. Since many exotic transients share some similar properties to SNe Ia, one may learn more about the physics of SNe Ia by observing their peculiar cousins.

Many of the transients in these classes are less luminous and faster than SNe Ia. Moreover, all appear to have a lower volumetric rate than SNe Ia (e.g. Foley et al. 2013). As a result, exotic thermonuclear transients are generally detected at a rate of $\lesssim$5 per cent that of SNe Ia in magnitude-limited surveys (Li et al. 2011). For the DES-SN survey, we therefore expect to detect $\sim$ 100 exotic thermonuclear transients. Because of their low luminosity, nearly all should be at $z \lesssim 0.1$. DES-SN has not yet spectroscopically identified any such transient.

10.4 Tidal disruption events

If a star comes sufficiently close to a massive black hole (MBH), the tidal forces will be strong enough to disrupt the star. If this occurs outside of the event horizon, it is possible that a luminous transient will be associated with the disruption. Rees (1988) first described this process, showing that for stars on bound orbits, that roughly half of the disrupted star would become unbound, while the other half would return on bound orbits, eventually accreting on to the MBH. This accretion should power a luminous transient similar to, but generally stronger than, an AGN flare.

TDEs are useful for detecting quiescent BHs, which is particularly important for determining the MBH occupation fraction in low-mass galaxies. Since the luminosity of a TDE is related to the mass of the MBH, a large sample of well-observed TDEs can be used to cleanly measure the MBH mass function. Furthermore, the TDE rate, especially in recently merged galaxies, can indicate the conditions of the nuclear star cluster and determine the importance of stellar scattering for MBH mergers.

There have been several TDE candidates discovered in the optical (e.g. van Velzen et al. 2011; Arcavi et al. 2014; Holoien et al. 2014), with the best-observed examples being discovered by PS1 (Gezari et al. 2012; Chornock et al. 2014) and ASAS-SN (Holoien et al. 2016). With multicolour light curves that cover the entire rise and decline, one can begin to disentangle parameters of the disrupted star (such as mass, composition, impact parameter, etc.) and the MBH mass. There have been few TDEs with good optical coverage on the rise, and additional data will be critical for understanding the physics of TDEs.

To date, DES-SN has detected a single TDE candidate (Foley et al. 2015). Based on current TDE rates (e.g. van Velzen & Farrar 2014), we expect one to five TDEs discovered in the DES-SN survey.

10.5 Gamma-ray bursts

We have initiated a programme to provide to the astronomical community in near-real time those data that are relevant to transients detected by other instruments. In its initial application, this programme entitled DESAlert (Poci et al. 2015) automatically receives VOEvent notices (Seaman et al. 2011) from the *Swift* satellite (Barthelmy et al. 2005) whenever its instruments detect a GRB. In response, DESAlert finds all objects within the DES catalogues within a pre-determined search radius of the GRB position, and disseminates information about these objects in a subsequent VOEvent notice of its own. Of particular relevance to follow-up observations of these GRBs, DESAlert identifies potential standard calibration stars (facilitating immediate relative photometry), as well as potential host galaxies (including magnitude, photometric redshift and morphological characteristics). The DESAlert service is expected to provide this information to the community for 1–2 dozen GRBs (all those occurring within the DES footprint) every year.

11 SUMMARY

In this overview paper, we have illustrated the legacy prospect of DES, beyond its primary goal for cosmological studies. DES is providing both a deep mapping of 5000 sq deg of the sky and a time-domain survey over 27 sq deg. Although optimized to measure and characterize DE, it has already yielded both expected and unexpected discoveries using initial SV data and the Y1 and Y2 data over most of the footprint (to about 40 per cent of the expected 5 yr magnitude depth).

We have highlighted some of the initial discoveries, from the Solar system to the high-redshift universe (see Table 1 for more details):

(i) 34 TNOs;

(ii) 17 new dwarf satellites of the Milky Way, and mapping of the LMC and its stellar population;

(iii) two published SLSNe, and more confirmed;

(iv) one published quasar at redshift $z > 6$, and more confirmed;

(v) two strongly lensed quasars.

The forecast for the complete 5 yr DES is very promising; for example, DES is likely to discover:

(i) many times more 'hot' TNOs than any previous survey;
(ii) more new dwarf satellites of the Milky Way, including even lower surface brightness objects than are currently known, as well as new stellar streams that probe the MW halo;
(iii) over 370 quasars at redshift $6 < z < 7$ and $\sim$ five at $z > 7$;
(iv) roughly 1000 strong lensing systems;
(v) possible detection of optical counterparts of GW events.

In addition, the cosmological probes of the wide-field DES, i.e. galaxy clustering, weak lensing and clusters, have already produced interesting results on galaxy biasing as a function of redshift, and on the profiles of galaxy versus DM in clusters. We expect that analysis of the full data set will allow tight constraints on the galaxy–halo connection in a broad range of environments and out to $z \sim 1$, and will produce new insights into galaxy and quasar evolution.

DES data are powerful not just on their own, but also in combination with other multiwavelength data (e.g. VISTA, SPT) and spectroscopy (e.g. OzDES, 2dFLens). The discoveries already made by DES using advanced statistical techniques also foretell the great discoveries ahead with the next generation of deeper and wider imaging surveys such as LSST, *Euclid* and WFIRST, combined with spectroscopic surveys such as DESI.

ACKNOWLEDGEMENTS

Funding for the DES Projects has been provided by the US Department of Energy, the US National Science Foundation, the Ministry of Science and Education of Spain, the Science and Technology Facilities Council of the United Kingdom, the Higher Education Funding Council for England, the National Center for Supercomputing Applications at the University of Illinois at Urbana-Champaign, the Kavli Institute of Cosmological Physics at the University of Chicago, the Center for Cosmology and Astro-Particle Physics at the Ohio State University, the Mitchell Institute for Fundamental Physics and Astronomy at Texas A&M University, Financiadora de Estudos e Projetos, Fundação Carlos Chagas Filho de Amparo à Pesquisa do Estado do Rio de Janeiro, Conselho Nacional de Desenvolvimento Científico e Tecnológico and the Ministério da Ciência, Tecnologia e Inovação, the Deutsche Forschungsgemeinschaft and the Collaborating Institutions in the Dark Energy Survey. The DES Data Management system is supported by the National Science Foundation under Grant Number AST-1138766.

The Collaborating Institutions are Argonne National Laboratory, the University of California at Santa Cruz, the University of Cambridge, Centro de Investigaciones Enérgeticas, Medioambientales y Tecnológicas-Madrid, the University of Chicago, University College London, the DES-Brazil Consortium, the University of Edinburgh, the Eidgenössische Technische Hochschule (ETH) Zürich, Fermi National Accelerator Laboratory, the University of Illinois at Urbana-Champaign, the Institut de Ciències de l'Espai (IEEC/CSIC), the Institut de Física d'Altes Energies, Lawrence Berkeley National Laboratory, the Ludwig-Maximilians Universität München and the associated Excellence Cluster Universe, the University of Michigan, the National Optical Astronomy Observatory, the University of Nottingham, the Ohio State University, the University of Pennsylvania, the University of Portsmouth, SLAC National Accelerator Laboratory, Stanford University, the University of Sussex and Texas A&M University.

OL acknowledges support from a European Research Council Advanced Grant FP7/291329. The DES participants from Spanish institutions are partially supported by MINECO under grants AYA2012-39559, ESP2013-48274, FPA2013-47986 and Centro de Excelencia Severo Ochoa SEV-2012-0234. Research leading to these results has received funding from the European Research Council under the European Union's Seventh Framework Programme (FP7/2007-2013) including ERC grant agreements 240672, 291329 and 306478.

We are grateful for the extraordinary contributions of our CTIO colleagues and the DECam Construction, Commissioning and Science Verification teams in achieving the excellent instrument and telescope conditions that have made this work possible. The success of this project also relies critically on the expertise and dedication of the DES Data Management group.

The VISTA Hemisphere Survey (VHS) is based on observations obtained as part of ESO Programme 179.A-2010 (PI: McMahon).

This paper has gone through internal review by the DES Collaboration.

REFERENCES

Aasi J. et al., 2014, ApJS, 211, 7
Abadie J. et al., 2010, Class. Quantum Grav., 27, 173001
Abbott B. P. et al., 2016, preprint (arXiv:1602.08492)
Abdalla F. B. et al., 2015, Proc. Sci., Advancing Astrophysics with the Square Kilometre Array (AASKA14). SISSA, Trieste, PoS#17
Agnello A., Kelly B. C., Treu T., Marshall P. J., 2015, MNRAS, 448, 1446
Ahn C. P. et al., 2012, ApJS, 203, 21
Allen S. W., Rapetti D. A., Schmidt R. W., Ebeling H., Morris R. G., Fabian A. C., 2008, MNRAS, 383, 879
Allen S. W., Evrard A. E., Mantz A. B., 2011, ARA&A, 49, 409
Allen L. et al., 2014, in American Astronomical Society, 46th Annual Meeting, Division for Planetary Sciences, Tucson, AZ, p. 414.01
Althaus L. G., Córsico A. H., Isern J., García-Berro E., 2010, A&AR, 18, 471
Angulo R., Fasiello M., Senatore L., Vlah Z., 2015, J. Cosmol. Astropart. Phys., 9, 029
Annis J. et al., 2016, preprint (arXiv:1602.04199)
Arcavi I. et al., 2014, ApJ, 793, 38
Arnaud M., Evrard A. E., 1999, MNRAS, 305, 631
Arnold T. J., Martini P., Mulchaey J. S., Berti A., Jeltema T. E., 2009, ApJ, 707, 1691
Assassi V., Baumann D., Green D., Zaldarriaga M., 2014, J. Cosmol. Astropart. Phys., 8, 56
Balbinot E., Santiago B. X., da Costa L. N., Makler M., Maia M. A. G., 2011, MNRAS, 416, 393
Balbinot E. et al., 2015, MNRAS, 449, 1129
Balbinot E. et al., 2016, ApJ, 820, 58
Banerji M., McMahon R. G., Hewett P. C., Alaghband-Zadeh S., Gonzalez-Solares E., Venemans B. P., Hawthorn M. J., 2012, MNRAS, 427, 2275
Banerji M., McMahon R. G., Hewett P. C., Gonzalez-Solares E., Koposov S. E., 2013, MNRAS, 429, L55
Banerji M. et al., 2015, MNRAS, 446, 2523
Bardeen J. M., Bond J. R., Kaiser N., Szalay A. S., 1986, ApJ, 304, 15
Barnes S. A., 2003, ApJ, 586, 464
Barnes S. A., 2007, ApJ, 669, 1167
Barth A. J. et al., 2015, ApJS, 217, 26
Barthelmy S. D. et al., 2005, Space Sci. Rev., 120, 143
Basri G., Marcy G. W., Graham J. R., 1996, ApJ, 458, 600
Batygin K., Brown M. E., 2016, AJ, 151, 22
Baugh C. M., Lacey C. G., Frenk C. S., Granato G. L., Silva L., Bressan A., Benson A. J., Cole S., 2005, MNRAS, 356, 1191
Bayliss M. B., Rigby J. R., Sharon K., Wuyts E., Florian M., Gladders M. D., Johnson T., Oguri M., 2014, ApJ, 790, 144
Bechtol K. et al., 2015, ApJ, 807, 50

Becker M. R. et al., 2007, ApJ, 669, 905
Belokurov V. et al., 2006, ApJ, 642, L137
Belokurov V., Evans N. W., Hewett P. C., Moiseev A., McMahon R. G., Sanchez S. F., King L. J., 2009, MNRAS, 392, 104
Benson A. J., Cole S., Frenk C. S., Baugh C. M., Lacey C. G., 2000, MNRAS, 311, 793
Bentz M. C., Katz S., 2015, PASP, 127, 67
Bentz M. C. et al., 2010, ApJ, 716, 993
Bentz M. C. et al., 2013, ApJ, 767, 149
Berger E., Fong W., Chornock R., 2013, ApJ, 774, L23
Bernardi M., Hyde J. B., Sheth R. K., Miller C. J., Nichol R. C., 2007, AJ, 133, 1741
Bernardi M., Meert A., Sheth R. K., Huertas-Company M., Maraston C., Shankar F., Vikram V., 2016, MNRAS, 455, 4122
Bernstein G., Khushalani B., 2000, AJ, 120, 3323
Bernstein J. P. et al., 2012, ApJ, 753, 152
Bildsten L., Shen K. J., Weinberg N. N., Nelemans G., 2007, ApJ, 662, L95
Blandford R. D., McKee C. F., 1982, ApJ, 255, 419
Blanton M. R., Moustakas J., 2009, ARA&A, 47, 159
Blazek J., Mandelbaum R., Seljak U., Nakajima R., 2012, J. Cosmol. Astropart. Phys., 5, 041
Bolzonella M. et al., 2010, A&A, 524, A76
Bouwens R. J. et al., 2010, ApJ, 725, 1587
Bouwens R. J. et al., 2015, ApJ, 803, 34
Bowler R. A. A. et al., 2014, MNRAS, 440, 2810
Boyle B. J., Terlevich R. J., 1998, MNRAS, 293, L49
Bradač M. et al., 2006, ApJ, 652, 937
Bradač M. et al., 2008a, ApJ, 681, 187
Bradač M., Allen S. W., Treu T., Ebeling H., Massey R., Morris R. G., von der Linden A., Applegate D., 2008b, ApJ, 687, 959
Bridle S., King L., 2007, New J. Phys., 9, 444
Bringmann T., Weniger C., 2012, Phys. Dark Universe, 1, 194
Brough S., Couch W. J., Collins C. A., Jarrett T., Burke D. J., Mann R. G., 2008, MNRAS, 385, L103
Brough S. et al., 2013, MNRAS, 435, 2903
Brown M. et al., 2014, Advancing Astrophysics with the Square Kilometre Array (AASKA14). SISSA, Trieste, PoS#23
Buckley-Geer E. J. et al., 2011, ApJ, 742, 48
Buitrago F., Trujillo I., Conselice C. J., Häußler B., 2013, MNRAS, 428, 1460
Cargile P. A., James D. J., 2010, AJ, 140, 677
Cargile P. A., James D. J., Jeffries R. D., 2010, ApJ, 725, L111
Carraro G., Lia C., 2000, A&A, 357, 977
Carrasco Kind M., Brunner R. J., 2013, MNRAS, 432, 1483
Carrasco Kind M., Brunner R. J., 2014, MNRAS, 442, 3380
Carrera R., Gallart C., Hardy E., Aparicio A., Zinn R., 2008, AJ, 135, 836
Carrera R., Gallart C., Aparicio A., Hardy E., 2011, AJ, 142, 61
Carretta E., Bragaglia A., Gratton R., Lucatello S., 2009, A&A, 505, 139
Cassano R. et al., 2013, ApJ, 777, 141
Chabrier G., Baraffe I., Allard F., Hauschildt P., 2000, ApJ, 542, 464
Chang C. et al., 2015, Phys. Rev. Lett., 115, 051301
Chang C. et al., 2016, MNRAS, 459, 3203
Chornock R. et al., 2014, ApJ, 780, 44
Cimatti A., 2006, Nuovo Cimento B, 121, 1383
Clerkin L., Kirk D., Lahav O., Abdalla F. B., Gaztañaga E., 2015, MNRAS, 448, 1389
Cole S., Kaiser N., 1989, MNRAS, 237, 1127
Collett T. E., 2015, ApJ, 811, 20
Collin S., Kawaguchi T., Peterson B. M., Vestergaard M., 2006, A&A, 456, 75
Conroy C., Wechsler R. H., Kravtsov A. V., 2007, ApJ, 668, 826
Conselice C. J., 2003, ApJS, 147, 1
Crocce M., Castander F. J., Gaztañaga E., Fosalba P., Carretero J., 2015, MNRAS, 453, 1513
Crocce M. et al., 2016, MNRAS, 455, 4301
Cuciti V., Cassano R., Brunetti G., Dallacasa D., Kale R., Ettori S., Venturi T., 2015, A&A, 580, A97
Da Costa G. S., Coleman M. G., 2008, AJ, 136, 506
Dall'Ora M. et al., 2004, ApJ, 610, 269
Dark Energy Survey Collaboration 2005, preprint (arXiv:astro-ph/0510346)
Dark Energy Survey Collaboration 2015, preprint (arXiv:1507.05552)
Dasyra K. et al., 2007, BAAS, 39, 144
Davis M., Geller M. J., 1976, ApJ, 208, 13
Davis T. et al., 2013, in American Astronomical Society Meeting Abstracts, Vol. 221, p. 106.02
Dawson K. S. et al., 2013, AJ, 145, 10
Day-Jones A. et al., 2013a, Mem. Soc. Astron. Ital., 84, 968
Day-Jones A. C. et al., 2013b, MNRAS, 430, 1171
de Jong J. T. A., Yanny B., Rix H.-W., Dolphin A. E., Martin N. F., Beers T. C., 2010, ApJ, 714, 663
de la Fuente Marcos C., de la Fuente Marcos R., 2014, MNRAS, 443, L59
De Lucia G., Blaizot J., 2007, MNRAS, 375, 2
Deb S., Goldberg D. M., Ramdass V. J., 2008, ApJ, 687, 39
Dekel A., Lahav O., 1999, ApJ, 520, 24
Del Moro A., Mateos S., Watson M. G., Akiyama M., 2008, in Lanteri L., Raiteri C. M., Capetti A., Rossi P., eds, Proc. 8th National Conference on AGN. Torini, Italy, p. 15
Desai S., Kahya E. O., Woodard R. P., 2008, Phys. Rev. D, 77, 124041
Di Matteo T., Springel V., Hernquist L., 2005, Nature, 433, 604
Diego J. M., Tegmark M., Protopapas P., Sandvik H. B., 2007, MNRAS, 375, 958
Dressler A., 1980, ApJ, 236, 351
Drlica-Wagner A. et al., 2015a, ApJ, 809, L4
Drlica-Wagner A. et al., 2015b, ApJ, 813, 109
Du C.-H., Wu Z.-Y., Ma J., Zhou X., 2008, Chin. J. Astron. Astrophys., 8, 566
Etherington J., Thomas D., 2015, MNRAS, 451, 5179
Evrard A. E., Arnault P., Huterer D., Farahi A., 2014, MNRAS, 441, 3562
Fan X. et al., 2001, AJ, 122, 2833
Fan X., Narayanan V. K., Strauss M. A., White R. L., Becker R. H., Pentericci L., Rix H.-W., 2002, AJ, 123, 1247
Fan X. et al., 2006, AJ, 132, 117
Ferrarese L., Merritt D., 2000, ApJ, 539, L9
Ferrarese L., Peterson B., Pogge R., Merritt D., Wandel A., 2001, Understanding Supermassive Black Holes and Their Host Galaxies. NOAO Proposal ID #2001B-0251
Flaugher B. et al., 2015, AJ, 150, 150
Foley R. J., 2015, MNRAS, 452, 2463
Foley R. J., Narayan G., Challis P. J., Filippenko A. V., Kirshner R. P., Silverman J. M., Steele T. N., 2010, ApJ, 708, 1748
Foley R. J. et al., 2013, ApJ, 767, 57
Foley R. J. et al., 2015, Astron. Telegram, 6877, 1
Franceschini A., Hasinger G., Miyaji T., Malquori D., 1999, MNRAS, 310, L5
Fry J. N., 1996, ApJ, 461, L65
Fry J. N., Gaztanaga E., 1993, ApJ, 413, 447
Furlanetto S. R., 2009, ApJ, 703, 702
Furlanetto S. R., Zaldarriaga M., Hernquist L., 2004, ApJ, 613, 1
Gal-Yam A., 2012, Science, 337, 927
Gallart C., Stetson P. B., Hardy E., Pont F., Zinn R., 2004, ApJ, 614, L109
Gallart C., Stetson P. B., Meschin I. P., Pont F., Hardy E., 2008, ApJ, 682, L89
Ganeshalingam M. et al., 2012, ApJ, 751, 142
Gavazzi R., Treu T., Koopmans L. V. E., Bolton A. S., Moustakas L. A., Burles S., Marshall P. J., 2008, ApJ, 677, 1046
Gavazzi R., Marshall P. J., Treu T., Sonnenfeld A., 2014, ApJ, 785, 144
Gaztanaga E., 1992, ApJ, 398, L17
Gaztañaga E., Scoccimarro R., 2005, MNRAS, 361, 824
Gebhardt K. et al., 2000, ApJ, 539, L13
Genzel R. et al., 2014, ApJ, 796, 7
Gerdes D. W. et al., 2016, AJ, 151, 39
Geringer-Sameth A., Walker M. G., Koushiappas S. M., Koposov S. E., Belokurov V., Torrealba G., Evans N. W., 2015, Phys. Rev. Lett., 115, 081101
Gerke B. F. et al., 2007, MNRAS, 376, 1425

Gezari S. et al., 2012, Nature, 485, 217
Giannantonio T. et al., 2016, MNRAS, 456, 3213
Girardi L., 1999, MNRAS, 308, 818
Goldstein D. A. et al., 2015, AJ, 150, 82
Gonzalez A. H., Zabludoff A. I., Zaritsky D., 2005, ApJ, 618, 195
Grier C. J. et al., 2012, ApJ, 755, 60
Gunn J. E., Peterson B. A., 1965, ApJ, 142, 1633
Guo H., Jing Y. P., 2009, ApJ, 698, 479
Haiman Z., Hui L., 2001, ApJ, 547, 27
Haines C. P., Smith G. P., Egami E., Okabe N., Takada M., Ellis R. S., Moran S. M., Umetsu K., 2009, MNRAS, 396, 1297
Haines C. P. et al., 2015, ApJ, 806, 101
Hansen S. M., Sheldon E. S., Wechsler R. H., Koester B. P., 2009, ApJ, 699, 1333
Hargis J. R., Willman B., Peter A. H. G., 2014, ApJ, 795, L13
Harris W. E., 1996, AJ, 112, 1487
Hartley W. G., Conselice C. J., Mortlock A., Foucaud S., Simpson C., 2015, MNRAS, 451, 1613
Harvey D., Massey R., Kitching T., Taylor A., Tittley E., 2015, Science, 347, 1462
Heymans C. et al., 2013, MNRAS, 432, 2433
Hicks A. K. et al., 2007, ApJ, 671, 1446
Hirata C. M., Mandelbaum R., Ishak M., Seljak U., Nichol R., Pimbblet K. A., Ross N. P., Wake D., 2007, MNRAS, 381, 1197
Holoien T. W.-S. et al., 2014, MNRAS, 445, 3263
Holoien T. W.-S. et al., 2016, MNRAS, 455, 2918
Holz D. E., Hughes S. A., 2005, ApJ, 629, 15
Hooper D., Linden T., 2015, J. Cosmol. Astropart. Phys., 9, 016
Hopkins P. F., Hernquist L., Cox T. J., Kereš D., 2008, ApJS, 175, 356
Horne K., Peterson B. M., Collier S. J., Netzer H., 2004, PASP, 116, 465
Ivezić Ž. et al., 2008, ApJ, 684, 287
James D. J. et al., 2010, A&A, 515, A100
Janka H.-T., Langanke K., Marek A., Martínez-Pinedo G., Müller B., 2007, Phys. Rep., 442, 38
Jarvis M. J. et al., 2013, MNRAS, 428, 1281
Jarvis M. et al., 2015, preprint (arXiv:1507.05603)
Jiménez-Vicente J., Mediavilla E., Kochanek C. S., Muñoz J. A., 2015, ApJ, 799, 149
Joachimi B., Bridle S. L., 2010, A&A, 523, A1
Joachimi B., Mandelbaum R., Abdalla F. B., Bridle S. L., 2011, A&A, 527, A26
Joachimi B. et al., 2015, Space Sci. Rev., 193, 1
Johansson P. H., Naab T., Ostriker J. P., 2012, ApJ, 754, 115
Jones L. R., Ponman T. J., Horton A., Babul A., Ebeling H., Burke D. J., 2003, MNRAS, 343, 627
Jurić M. et al., 2008, ApJ, 673, 864
Kaiser N., 1984, ApJ, 284, L9
Kalirai J. S., Ventura P., Richer H. B., Fahlman G. G., Durrell P. R., D'Antona F., Marconi G., 2001, AJ, 122, 3239
Kasen D., Bildsten L., 2010, ApJ, 717, 245
Kaspi S. et al., 2002, ApJ, 574, 643
Kessler R. et al., 2015, AJ, 150, 172
Kiessling A. et al., 2015, Space Sci. Rev., 193, 67
Kilic M. et al., 2006, AJ, 131, 582
Kim D., Jerjen H., 2015, ApJ, 808, L39
King A. L. et al., 2015, MNRAS, 453, 1701
Kinman T. D., Stryker L. L., Hesser J. E., Graham J. A., Walker A. R., Hazen M. L., Nemec J. M., 1991, PASP, 103, 1279
Kirk D. et al., 2015, Space Sci. Rev., 193, 139
Kirk D. et al., 2016, MNRAS, 459, 21
Knapp G. R. et al., 2004, AJ, 127, 3553
Kollmeier J. A. et al., 2006, ApJ, 648, 128
Koposov S. et al., 2008, ApJ, 686, 279
Koposov S. E., Rix H.-W., Hogg D. W., 2010, ApJ, 712, 260
Koposov S. E., Belokurov V., Torrealba G., Evans N. W., 2015a, ApJ, 805, 130
Koposov S. E. et al., 2015b, ApJ, 811, 62
Krick J. E., Bernstein R. A., Pimbblet K. A., 2006, AJ, 131, 168
Kubik D., 2007, M.S. thesis, Northern Illinois University
Kubo J. M. et al., 2010, ApJ, 724, L137
Kuehn C. A. et al., 2013, AJ, 145, 160
Küpper A. H. W., Balbinot E., Bonaca A., Johnston K. V., Hogg D. W., Kroupa P., Santiago B. X., 2015, ApJ, 803, 80
Lahav O., Kiakotou A., Abdalla F. B., Blake C., 2010, MNRAS, 405, 168
Leistedt B. et al., 2015, preprint (arXiv:1507.05647)
Li W. et al., 2011, MNRAS, 412, 1441
Lidman C. et al., 2012, MNRAS, 427, 550
LIGO Scientific Collaboration Virgo Collaboration, 2016, Phys. Rev. Lett., 116, 061102
LIGO Scientific Collaboration 2013, preprint (arXiv:1304.0670)
Limousin M. et al., 2007, ApJ, 668, 643
Lunnan R. et al., 2014, ApJ, 787, 138
Lunnan R. et al., 2015, ApJ, 804, 90
Luque E. et al., 2016, MNRAS, 458, 603
Mackey A. D., Gilmore G. F., 2004, MNRAS, 352, 153
Mackey A. D., Koposov S. E., Erkal D., Belokurov V., Da Costa G. S., Gómez F. A., 2016, MNRAS, 459, 239
McConnachie A. W., 2012, AJ, 144, 4
McConnell N. J., Ma C.-P., Murphy J. D., Gebhardt K., Lauer T. R., Graham J. R., Wright S. A., Richstone D. O., 2012, ApJ, 756, 179
McDonald P., Roy A., 2009, J. Cosmol. Astropart. Phys., 8, 20
McDonald M. et al., 2012, Nature, 488, 349
McDonald M. et al., 2013, ApJ, 774, 23
McDonald M. et al., 2014, ApJ, 794, 67
McGreer I. D. et al., 2013, ApJ, 768, 105
McLure R. J., Dunlop J. S., 2004, in Mújica R., Maiolino R., eds., Multi-wavelength AGN Surveys. p. 389
McLure R. J. et al., 2011, MNRAS, 418, 2074
McMahon R. G., Banerji M., Gonzalez E., Koposov S. E., Bejar V. J., Lodieu N., Rebolo R., VHS Collaboration, 2013, The Messenger, 154, 35
Maddox N., Hewett P. C., Warren S. J., Croom S. M., 2008, MNRAS, 386, 1605
Maddox N., Hewett P. C., Péroux C., Nestor D. B., Wisotzki L., 2012, MNRAS, 424, 2876
Mandelbaum R., Slosar A., Baldauf T., Seljak U., Hirata C. M., Nakajima R., Reyes R., Smith R. E., 2013, MNRAS, 432, 1544
Mann R. G., Peacock J. A., Heavens A. F., 1998, MNRAS, 293, 209
Mao Y.-Y., Williamson M., Wechsler R. H., 2015, ApJ, 810, 21
Maraston C., Pforr J., Renzini A., Daddi E., Dickinson M., Cimatti A., Tonini C., 2010, MNRAS, 407, 830
Maraston C. et al., 2013, MNRAS, 435, 2764
Marchesini D., van Dokkum P. G., Förster Schreiber N. M., Franx M., Labbé I., Wuyts S., 2009, ApJ, 701, 1765
Marino A. F., Villanova S., Piotto G., Milone A. P., Momany Y., Bedin L. R., Medling A. M., 2008, A&A, 490, 625
Markevitch M., 1998, ApJ, 504, 27
Markevitch M., Gonzalez A. H., Clowe D., Vikhlinin A., Forman W., Jones C., Murray S., Tucker W., 2004, ApJ, 606, 819
Marshall P. J. et al., 2016, MNRAS, 455, 1171
Martin N. F. et al., 2015, ApJ, 804, L5
Martini P., 2004, Coevolution of Black Holes and Galaxies, Cambridge Univ. Press, Cambridge, p. 169
Martini P., Weinberg D. H., 2001, ApJ, 547, 12
Martini P., Sivakoff G. R., Mulchaey J. S., 2009, ApJ, 701, 66
Martini P. et al., 2013, ApJ, 768, 1
Mauduit J.-C. et al., 2012, PASP, 124, 714
Meiksin A. A., 2009, Rev. Mod. Phys., 81, 1405
Merloni A., Rudnick G., Di Matteo T., 2004, MNRAS, 354, L37
Merten J., Cacciato M., Meneghetti M., Mignone C., Bartelmann M., 2009, A&A, 500, 681
Millis R. L., Buie M. W., Wasserman L. H., Elliot J. L., Kern S. D., Wagner R. M., 2002, AJ, 123, 2083
Mo H. J., White S. D. M., 1996, MNRAS, 282, 347
Monaco P., Murante G., Borgani S., Fontanot F., 2006, ApJ, 652, L89
Moraux E., Kroupa P., Bouvier J., 2004, A&A, 426, 75

More A., Cabanac R., More S., Alard C., Limousin M., Kneib J.-P., Gavazzi R., Motta V., 2012, ApJ, 749, 38
Mortlock D. J. et al., 2011, Nature, 474, 616
Mortlock A. et al., 2013, MNRAS, 433, 1185
Natarajan P., Kneib J.-P., Smail I., Ellis R. S., 1998, ApJ, 499, 600
Natarajan P., Loeb A., Kneib J.-P., Smail I., 2002, ApJ, 580, L17
Navarro J. F., Frenk C. S., White S. D. M., 1997, ApJ, 490, 493
Neill J. D. et al., 2011, ApJ, 727, 15
Nicholl M. et al., 2014, MNRAS, 444, 2096
Nicholl M. et al., 2015, ApJ, 807, L18
Nierenberg A. M., Treu T., Wright S. A., Fassnacht C. D., Auger M. W., 2014, MNRAS, 442, 2434
Nishizawa A., Nakamura T., 2014, Phys. Rev. D, 90, 044048
Nord B. et al., 2015, preprint (arXiv:1512.03062)
Norris R. P. et al., 2011, Publ. Astron. Soc. Aust., 28, 215
Nugent P. et al., 2006, ApJ, 645, 841
Nusser A., Davis M., 1994, ApJ, 421, L1
Oguri M., Marshall P. J., 2010, MNRAS, 405, 2579
Oguri M. et al., 2009, ApJ, 699, 1038
Oguri M., Rusu C. E., Falco E. E., 2014, MNRAS, 439, 2494
Onken C. A. et al., 2014, ApJ, 791, 37
Palmese A. et al., 2016, preprint (arXiv:1601.00589)
Pancoast A., Brewer B. J., Treu T., 2014, MNRAS, 445, 3055
Pan Y.-C. et al., 2015, Astron. Telegram, 8424, 1
Papadopoulos A. et al., 2015, MNRAS, 449, 1215
Peng C. Y., Impey C. D., Rix H.-W., Kochanek C. S., Keeton C. R., Falco E. E., Lehár J., McLeod B. A., 2006, ApJ, 649, 616
Peng Y.-j. et al., 2010, ApJ, 721, 193
Perets H. B. et al., 2010, Nature, 465, 322
Peterson B. M., 1993, PASP, 105, 247
Pieres A. et al., 2015, preprint (arXiv:1512.01032)
Pierini D., Zibetti S., Braglia F., Böhringer H., Finoguenov A., Lynam P. D., Zhang Y.-Y., 2008, A&A, 483, 727
Poci A. et al., 2015, preprint (arXiv:1504.02996)
Poindexter S., Morgan N., Kochanek C. S., 2008, ApJ, 673, 34
Pozzetti L. et al., 2010, A&A, 523, A13
Quimby R. M., Yuan F., Akerlof C., Wheeler J. C., 2013, MNRAS, 431, 912
Raouf M., Khosroshahi H. G., Ponman T. J., Dariush A. A., Molaeinezhad A., Tavasoli S., 2014, MNRAS, 442, 1578
Reed S. L. et al., 2015, MNRAS, 454, 3952
Rees M. J., 1988, Nature, 333, 523
Reylé C., Marshall D. J., Robin A. C., Schultheis M., 2009, A&A, 495, 819
Rhoads J. E. et al., 2014, ApJ, 787, 8
Richards G. et al., 2006, in Armus L., Reach W. T., eds, ASP Conf. Ser. Vol. 357, The Spitzer Space Telescope: New Views of the Cosmos. Astron. Soc. Pac., San Francisco, p. 261
Robichon N., Arenou F., Mermilliod J.-C., Turon C., 1999, A&A, 345, 471
Rocha-Pinto H. J., Majewski S. R., Skrutskie M. F., Crane J. D., Patterson R. J., 2004, ApJ, 615, 732
Rossetto B. M. et al., 2011, AJ, 141, 185
Rusu C. E. et al., 2016, MNRAS, 458, 2
Rykoff E. S. et al., 2016, preprint (arXiv:1601.00621)
Saintonge A. et al., 2013, ApJ, 778, 2
Sako M. et al., 2014, preprint (arXiv:1401.3317)
Sánchez C. et al., 2014, MNRAS, 445, 1482
Saumon D., Marley M. S., 2008, ApJ, 689, 1327
Schechter P. L., Pooley D., Blackburne J. A., Wambsganss J., 2014, ApJ, 793, 96
Schmidt M., Schneider D. P., Gunn J. E., 1995, AJ, 110, 68
Schutz B. F., 1986, Nature, 323, 310
Scovacricchi D., Nichol R. C., Bacon D., Sullivan M., Prajs S., 2016, MNRAS, 456, 1700
Seaman R. et al., 2011, Sky Event Reporting Metadata Version 2.0, preprint (arXiv:1110.0523)
Shankar F., Crocce M., Miralda-Escudé J., Fosalba P., Weinberg D. H., 2010, ApJ, 718, 231
Sharma S., Johnston K. V., Majewski S. R., Muñoz R. R., Carlberg J. K., Bullock J., 2010, ApJ, 722, 750
Shen Y. et al., 2007, AJ, 133, 2222
Silverman J. D. et al., 2008, ApJ, 679, 118
Simon J. D. et al., 2015, ApJ, 808, 95
Singh S., Mandelbaum R., More S., 2015, MNRAS, 450, 2195
Sluse D. et al., 2011, A&A, 528, A100
Smartt S. J., 2009, ARA&A, 47, 63
Smith M. et al., 2016, ApJ, 818, L8
Soares-Santos M. et al., 2016, preprint (arXiv:1602.04198)
Sollima A., Cacciari C., Arkharov A. A. H., Larionov V. M., Gorshanov D. L., Efimova N. V., Piersimoni A., 2008, MNRAS, 384, 1583
Sonnenfeld A., Treu T., Gavazzi R., Marshall P. J., Auger M. W., Suyu S. H., Koopmans L. V. E., Bolton A. S., 2012, ApJ, 752, 163
Soumagnac M. T. et al., 2015, MNRAS, 450, 666
Stanway E. R., Bunker A., McMahon R. G., 2003, Ap&SS, 284, 381
Stauffer J. R., Schultz G., Kirkpatrick J. D., 1998, ApJ, 499, L199
Steidel C. C., Pettini M., Hamilton D., 1995, AJ, 110, 2519
Suchyta E. et al., 2016, MNRAS, 457, 786
Suyu S. H. et al., 2013, ApJ, 766, 70
Tanvir N. R., Levan A. J., Fruchter A. S., Hjorth J., Hounsell R. A., Wiersema K., Tunnicliffe R. L., 2013, Nature, 500, 547
Tegmark M., Peebles P. J. E., 1998, ApJ, 500, L79
Tejos N. et al., 2016, MNRAS, 455, 2662
Thomas S. A., Abdalla F. B., Lahav O., 2011, MNRAS, 412, 1669
Tinker J. L., Robertson B. E., Kravtsov A. V., Klypin A., Warren M. S., Yepes G., Gottlöber S., 2010, ApJ, 724, 878
Tollerud E. J., Bullock J. S., Strigari L. E., Willman B., 2008, ApJ, 688, 277
Tremaine S. et al., 2002, ApJ, 574, 740
Troxel M. A., Ishak M., 2015, Phys. Rep., 558, 1
Trujillo C. A., Sheppard S. S., 2014, Nature, 507, 471
Urrutia T., Lacy M., Becker R. H., 2008, ApJ, 674, 80
van Haarlem M. P. et al., 2013, A&A, 556, A2
van Oirschot P., Nelemans G., Toonen S., Pols O., Brown A. G. A., Helmi A., Portegies Zwart S., 2014, A&A, 569, A42
van Velzen S., Farrar G. R., 2014, ApJ, 792, 53
van Velzen S. et al., 2011, ApJ, 741, 73
Veron-Cetty M.-P., Veron P., 1993, ESO Scientific Report, A Catalogue of Quasars and Active Nuclei. European Southern Observatory, Garching
Vestergaard M., Osmer P. S., 2009, ApJ, 699, 800
Vestergaard M., Peterson B. M., 2006, ApJ, 641, 689
Vikram V. et al., 2015, Phys. Rev. D, 92, 022006
von der Linden A., Best P. N., Kauffmann G., White S. D. M., 2007, MNRAS, 379, 867
Walker A. R., 1992, AJ, 103, 1166
Walker M. G., Mateo M., Olszewski E. W., Bailey J. I., III, Koposov S. E., Belokurov V., Evans N. W., 2015, ApJ, 808, 108
Walsh S. M., Willman B., Jerjen H., 2009, AJ, 137, 450
Warren S. J., Hewett P. C., Osmer P. S., 1994, ApJ, 421, 412
Wetzel A. R., Tinker J. L., Conroy C., van den Bosch F. C., 2013, MNRAS, 432, 336
White S. D. M., 2007, Rep. Prog. Phys., 70, 883
White R. L., Helfand D. J., Becker R. H., Gregg M. D., Postman M., Lauer T. R., Oegerle W., 2003, AJ, 126, 706
White M., Martini P., Cohn J. D., 2008, MNRAS, 390, 1179
Whittaker L., Brown M. L., Battye R. A., 2015, MNRAS, 451, 383
Willman B., Governato F., Wadsley J., Quinn T., 2004, MNRAS, 355, 159
Willman B. et al., 2005, ApJ, 626, L85
Willott C. J. et al., 2010, AJ, 139, 906
Willott C. J. et al., 2013, AJ, 145, 4
Woosley S. E., 2010, ApJ, 719, L204
Woosley S. E., Bloom J. S., 2006, ARA&A, 44, 507
Yanny B. et al., 2000, ApJ, 540, 825
Yoon J. H., Johnston K. V., Hogg D. W., 2011, ApJ, 731, 58
Yuan F. et al., 2015, MNRAS, 452, 3047
Zehavi I., Zheng Z., Weinberg D., Blanton M., 2011, in Galaxy Formation. Durham, p. 140P
Zhang Z. H. et al., 2009, A&A, 497, 619

Zhang Y. et al., 2016, ApJ, 816, 98
Zibetti S., White S. D. M., Schneider D. P., Brinkmann J., 2005, MNRAS, 358, 949

[1]*Cerro Tololo Inter-American Observatory, National Optical Astronomy Observatory, Casilla 603, La Serena, Chile*
[2]*Department of Physics & Astronomy, University College London, Gower Street, London WC1E 6BT, UK*
[3]*Institut de Física d'Altes Energies (IFAE), The Barcelona Institute of Science and Technology, Campus UAB, E-08193 Bellaterra (Barcelona), Spain*
[4]*Fermi National Accelerator Laboratory, PO Box 500, Batavia, IL 60510, USA*
[5]*Department of Physics, ETH Zurich, Wolfgang-Pauli-Strasse 16, CH-8093 Zurich, Switzerland*
[6]*Institute of Cosmology & Gravitation, University of Portsmouth, Portsmouth PO1 3FX, UK*
[7]*Department of Physics, University of Surrey, Guildford GU2 7XH, UK*
[8]*Kavli Institute for Cosmology, University of Cambridge, Madingley Road, Cambridge CB3 0HA, UK*
[9]*Institute of Astronomy, University of Cambridge, Madingley Road, Cambridge CB3 0HA, UK*
[10]*Wisconsin IceCube Particle Astrophysics Center (WIPAC), Madison, WI 53703, USA*
[11]*Department of Physics, University of Wisconsin-Madison, Madison, WI 53706, USA*
[12]*Sorbonne Universités, UPMC Univ Paris 06, UMR 7095, Institut d'Astrophysique de Paris, F-75014 Paris, France*
[13]*CNRS, UMR 7095, Institut d'Astrophysique de Paris, F-75014 Paris, France*
[14]*Department of Physics and Astronomy, University of Pennsylvania, Philadelphia, PA 19104, USA*
[15]*Center for Cosmology and Astro-Particle Physics, The Ohio State University, Columbus, OH 43210, USA*
[16]*Institut de Física d'Altes Energies, Universitat Autònoma de Barcelona, E-08193 Bellaterra, Barcelona, Spain*
[17]*Jodrell Bank Centre for Astrophysics, School of Physics and Astronomy, University of Manchester, Oxford Road, Manchester M13 9PL, UK*
[18]*Department of Physics, University of Illinois, 1110 W. Green St., Urbana, IL 61801, USA*
[19]*National Center for Supercomputing Applications, 1205 West Clark St., Figure, IL 61801, USA*
[20]*Kavli Institute for Particle Astrophysics & Cosmology, PO Box 2450, Stanford University, Stanford, CA 94305, USA*
[21]*SLAC National Accelerator Laboratory, Menlo Park, CA 94025, USA*
[22]*ICRA, Centro Brasileiro de Pesquisas Físicas, Rua Dr. Xavier Sigaud 150, CEP 22290-180, Rio de Janeiro, RJ, Brazil*
[23]*Dipartimento di Fisica e Scienze della Terra, Università degli Studi di Ferrara, Via Saragat 1, I-44122 Ferrara, Italy*
[24]*Observatório Nacional, Rua Gal. José Cristino 77, Rio de Janeiro, RJ 20921-400, Brazil*
[25]*Laboratório Interinstitucional de e-Astronomia – LIneA, Rua Gal. José Cristino 77, Rio de Janeiro, RJ 20921-400, Brazil*
[26]*Institute of Astronomy, ETH Zurich, CH-8093 Zurich, Switzerland*
[27]*Department of Astronomy, University of Illinois, 1002 W. Green Street, Urbana, IL 61801, USA*
[28]*Institut de Ciències de l'Espai, IEEC-CSIC, Campus UAB, Carrer de Can Magrans, s/n, E-08193 Bellaterra, Barcelona, Spain*
[29]*School of Physics & Astronomy, University of Nottingham, Nottingham NG7 2RD, UK*
[30]*School of Mathematics and Physics, University of Queensland, QLD 4072, Australia*
[31]*Excellence Cluster Universe, Boltzmannstr. 2, D-85748 Garching, Germany*
[32]*Faculty of Physics, Ludwig-Maximilians University, Scheinerstr. 1, D-81679 Munich, Germany*
[33]*Kavli Institute for Cosmological Physics, University of Chicago, Chicago, IL 60637, USA*
[34]*Department of Astronomy and Astrophysics, University of Chicago, 5640 South Ellis Avenue, Chicago, IL 60637, USA*
[35]*Department of Physics, University of Michigan, Ann Arbor, MI 48109, USA*
[36]*Department of Astronomy, University of Michigan, Ann Arbor, MI 48109, USA*
[37]*Instituto de Física Teórica IFT-UAM/CSIC, Universidad Autónoma de Madrid, E-28049 Madrid, Spain*
[38]*Department of Astronomy, University of California, Berkeley, 501 Campbell Hall, Berkeley, CA 94720, USA*
[39]*Institució Catalana de Recerca i Estudis Avançats, E-08010 Barcelona, Spain*
[40]*Department of Physics, The Ohio State University, Columbus, OH 43210, USA*
[41]*Department of Physics and Santa Cruz Institute for Particle Physics, University of California, Santa Cruz, CA 95064, USA*
[42]*Australian Astronomical Observatory, North Ryde, NSW 2113, Australia*
[43]*George P. and Cynthia Woods Mitchell Institute for Fundamental Physics and Astronomy, and Department of Physics and Astronomy, Texas A&M University, College Station, TX 77843, USA*
[44]*Departamento de Física Matemática, Instituto de Física, Universidade de São Paulo, CP 66318, CEP 05314-970 São Paulo, Brazil*
[45]*Department of Astronomy, The Ohio State University, Columbus, OH 43210, USA*
[46]*Department of Astrophysical Sciences, Princeton University, Peyton Hall, Princeton, NJ 08544, USA*
[47]*Max Planck Institute for Extraterrestrial Physics, Giessenbachstrasse, D-85748 Garching, Germany*
[48]*School of Sciences, European University Cyprus, 6 Diogenis Str., Engomi, 1516 Nicosia, Cyprus*
[49]*Jet Propulsion Laboratory, California Institute of Technology, 4800 Oak Grove Dr., Pasadena, CA 91109, USA*
[50]*Department of Physics and Astronomy, Pevensey Building, University of Sussex, Brighton BN1 9QH, UK*
[51]*Department of Physics, University of Arizona, 1118 E 4th St, Tucson, AZ 85721, USA*
[52]*Centro de Investigaciones Energéticas, Medioambientales y Tecnológicas (CIEMAT), Madrid, Spain*
[53]*Instituto de Física, UFRGS, Caixa Postal 15051, Porto Alegre, RS 91501-970, Brazil*
[54]*Brookhaven National Laboratory, Bldg 510, Upton, NY 11973, USA*
[55]*School of Physics and Astronomy, University of Southampton, Southampton SO17 1BJ, UK*
[56]*National Center for Supercomputing Applications, 1205 West Clark St, Urbana, IL 61801, USA*
[57]*South East Physics Network (www.sepnet.ac.uk), UK*
[58]*Lawrence Berkeley National Laboratory, 1 Cyclotron Road, Berkeley, CA 94720, USA*
[59]*Argonne National Laboratory, 9700 South Cass Avenue, Lemont, IL 60439, USA*
[60]*Universitäts-Sternwarte, Fakultät für Physik, Ludwig-Maximilians Universität München, Scheinerstr. 1, D-81679 München, Germany*

This paper has been typeset from a TEX/LATEX file prepared by the author.